SYNTHESIS OF SILICA NANOSTRUCTURES BY USING WET-CHEMISTRY METHODS

By

HENAN ZHANG

A dissertation submitted to the Graduate Faculty in Chemistry in partial fulfillment of the requirements for the degree of Doctor of Philosophy, The City University of New York

2013

This manuscript has been read and accepted for the Graduate Faculty in Chemistry
In satisfaction of the dissertation requirement for the degree of Doctor of Philosophy.

	Dr. Daniel L. Akins
Date	Chair of Examining Committee
	Dr. Maria Tamargo
Date	Executive Officer

Dr. Daniel L. Akins

Dr. Charles M. Drain

Dr. John R. Lombardi

Dr. Aidong Sheng

Supervisory Committee

THE CITY UNIVERSITY OF NEW YORK

Abstract

SYNTHESIS OF SILICA NANOSTRUCTURES BY USING WET-CHEMISTRY METHODS

By

Henan Zhang

Advisor: Prof. Daniel L. Akins

For the sol-gel synthesis of silica particles under high pH catalytic conditions (pH>12) in water/ethanol solvent, we have deduced that the competing dynamics of chemical etching and sol-gel formation can explain the types of silica particles formed and their morphologies. We have demonstrated that emulsion droplets that are generated by adding tetraethyl orthosilicate (TEOS) to a water-ethanol solution serve as soft templates for hollow spherical silica (1~2 μm). And if the emulsion is converted by the sol-gel process, one finds that suspended solid silica spheres of diameter of ~900 nm are formed. Moreover, several other factors are found to play fundamental roles in determining the final morphologies of silica particles, such as by variation of the pH (in our case, using OH^-) to a level where condensation dominates; by changing the volume ratios of water/ethanol; and using an emulsifier (specifically, CTAB).

For a sol-gel process occurring in a water/oil (w/o) system, the self-assembly of silica nuclei can be controlled by close control of synthesis conditions. We have synthesized ellipsoidal or spherical silica particles by a template-free scheme that involves controlling surface tension on silica nuclei through via use of different volume ratios of a w/o micellar system.

We have utilized wet-chemical etching of ellipsoidal silica nanoparticles to form silica

nanoshells of a range of elliptical morphologies, with the thicknesses of the ellipsoidal silica nanoshells controlled through via variation of synthesis conditions. A mechanism has been proposed to explain how the nanoshells are formed, and we demonstrate that the porosity of the silica ellipsoid plays a role in generating silica shells. Moreover, silica materials with the unique structures might be adjusted to meet practical application requirements.

Acknowledgments

In retrospect of the past years in the City College of the City University of New York, there are countless people to whom I owe a debt of gratitude. Without their advice, guidance, assistance and encouragement, I would never be capable to accomplish this academic goal. Although it seems like a challenge of naming each and every of them, I truly wonder to express my in-depth gratitude to all of them. First and most important, I would like to thank my mentor, Prof. Daniel L. Akins, for his advice and guidance. I also thank my thesis committee members, Prof. John R. Lombardi, Prof. Charles M. Drain, and Prof. Aidong Shen.

I would like to thank many members of the Chemistry program at the City University of New York, the Graduate School, and the department of Chemistry at CCNY, including faculties, staffs and students, for providing a friendly working environment. My special gratitude is for our program administrator, Ms. Diane Beckford; and my lab mates, Dr. Huijun Jiang, Dr. Danh Ng uyen-Thanh, Dr. Yi Zhou, Mr. Yu Zhao, Mr. Yueru Li and Ms. Deon Hines. I am grateful to many colleagues, for the assistance of my research and the great friendship, who involve Prof. Jay W. Lee, Prof. Stephen O'Brien, Prof. Teresa J. Bandosz, Prof. Limin Huang, Dr. Shuangyi Liu, Dr. Junshe Zhang and etcetera.

My sincere gratitude is shown to my family, my parents Mr. Jifu Zhang and Mrs. Xiaohui Sun, my wife Chunxiao Fu, my son Derek, and my daughter Claire. They are always being on my side, warming my heart, and giving me unconditional love and encouragement.

I hope that this opportunity would express my gratitude for all the kindness, friendship and encouragement. Thanks, again.

This work is dedicated to whom I love with all my heart and soul

My wife Chunxiao Fu

Table of Contents

List of figures

List of tables and scheme

Chapter 1: Introduction

1.1 Overview and motivation

Nanotechnology, associated with the manipulation of matters at dimensions from a few angstroms (Å) to about 1000 Å, has garnered a great deal of attention from scientists in both academia and industry. Nanotechnology is the study and application of extremely small things in the nanorealm and can be used across all the other science fields. The potential applications of nanotechnology are debated by scientific researchers. Nanotechnology is able to create and exploit new materials on nanoscale, and extend conventional device physics to completely new approaches on the basis of molecular self-assembly. With the development of nanotechnology, nanomaterials enabling unique applications created for growing practical requirements are increasing being sought-after.

Silica nanomaterials have proven themselves to be of great interest from a basic science perspective as well as because of crucial roles such materials play in everyday commercial applications, for example, energy conversion and storage device, and drug delivery medium [1-4]. In particular, silica colloids on the nanometre length scale with the well-defined compositional and morphological control have proven to be imperative for enabling controlled porosity, solvent compatibility, and processability. A broad spectrum of synthesis protocols has been utilized to create morphologically different silica materials (i.e. spherical, ellipsoidal, and cubic) [5-10]. However, it is to be noted that, although the synthesis approaches for the formation of silica nanomaterials have been developed; it is of significance to better understand the basic science of silica, in order to form silica nanostructures with potential applications.

For these reason, the objective of the present thesis is to improve understanding the chemistry of

silica, and develop facile synthesis approaches for the formation of silica nanostructures with controlled morphologies and sizes.

1.2 Background

1.2.1 Sol-gel process

The sol-gel process is a wet-chemical technique, which is utilized for the fabrication of both glassy and ceramic materials. The observation of hydrolysis and polymerization of tetraethyel orthosicliate (TEOS) can be traced back in the mid-1980s, which led to the formation of silica fibres. In the last decades, silica nanomaterials, exhibiting potential use in energy storage, catalysis and drug delivery, became promising for a sustainable future; as a result, the research realm related to silica was paid ever-growing attentions. In our sol-gel process, TEOS is served as silica source, via undergoing the hydrolysis and polymerization reactions, leading to the formation of silica colloids [11].

As shown in formula (1), the alkyl groups of TEOS, -OR readily react with water (H_2O), which results in -OH. Such process is called hydrolysis.

$$Si(OR)_4 + H_2O \rightarrow HO\text{-}Si(OR)_3 + R\text{-}OH \quad (1)$$

When the hydrolysis proceeds completely, all of the -OR groups should be replaced by -OH groups, as indicated in formula (2).

$$Si(OR)_4 + 4\ H_2O \rightarrow Si(OH)_4 + 4\ R\text{-}OH \quad (2)$$

However, when hydrolysis proceeds partially, intermediate species [$(OR)_2$-Si-$(OH)_2$] or [$(OR)_3$-Si-(OH)] would be considered as results. Additionally, as shown in formula (3) or (4), two partially hydrolyzed or unhydrolyzed TEOS molecules can reaction as linkage in a condensation reaction to generate a siloxane [Si-O-Si] bond, at the same time, liberate small molecules, i.e. H-

O-H or R-OH.

$$(OR)_3\text{-Si-OH} + \text{HO–Si-}(OR)_3 \rightarrow [(OR)_3\text{Si-O-Si}(OR)_3] + \text{H-O-H} \quad (3)$$

Or

$$(OR)_3\text{-Si-OR} + \text{HO-Si-}(OR)_3 \rightarrow [(OR)_3\text{Si-O-Si}(OR)_3] + \text{R-OH} \quad (4)$$

As accompanied with the production of H-O-H and R-O-H species, the condensation reaction can generate silicon continuously containing molecules by proceeding polymerization (polycondensation), which results in the formation of network macromolecules with diverse dimensionalities.

Thus, the basic science perspective of the sol-gel process, which associates with hydrolysis, condensation and polymerization, are crucial for material design of silica materials.

1.2.2 Micelle and surfactant

A micelle is defined as an aggregate of well-dispersed surfactant molecules in a liquid colloid. As early as 1913, James William Mabain [12] postulated the existence of highly mobile clusters in sodium palmitate solutions, and named them micelles. It was known that, the formation of micelle is considered as an assembly of surfactant molecules; and, the promise of the formation of micelle is when the concentration of surfactant molecules is greater than the critical micelle concentration (CMC), as well as the temperature of the system is greater than the critical micelle temperature. Generally, micelle is classified as normal phase micelle (oil-in-water micelle) and inverse micelle (water-in-oil micelle). A typical oil-in-water micelle forms an aggregate with the hydrophilic "head" regions in contact with surrounding water, sequestering the hydrophobic tail regions in the centre, as indicated in Fig. 1-1 [13]. In contrast, a water-in-oil micelle is aggregated as the hydrophobic "head" regions in contact with surrounding "oil", sequestering the

hydrophilic tails from the surrounding. It is to be noted that, the formation of differently structural micelles is explained by the perspective of solvation and energy. Normally, the shape of micelles is in spherical; however, a variety of other shapes, such as cylinder and bilayers, can be varied by controlling the geometries of the surfactant molecules and the nature of the surrounding solution conditions.

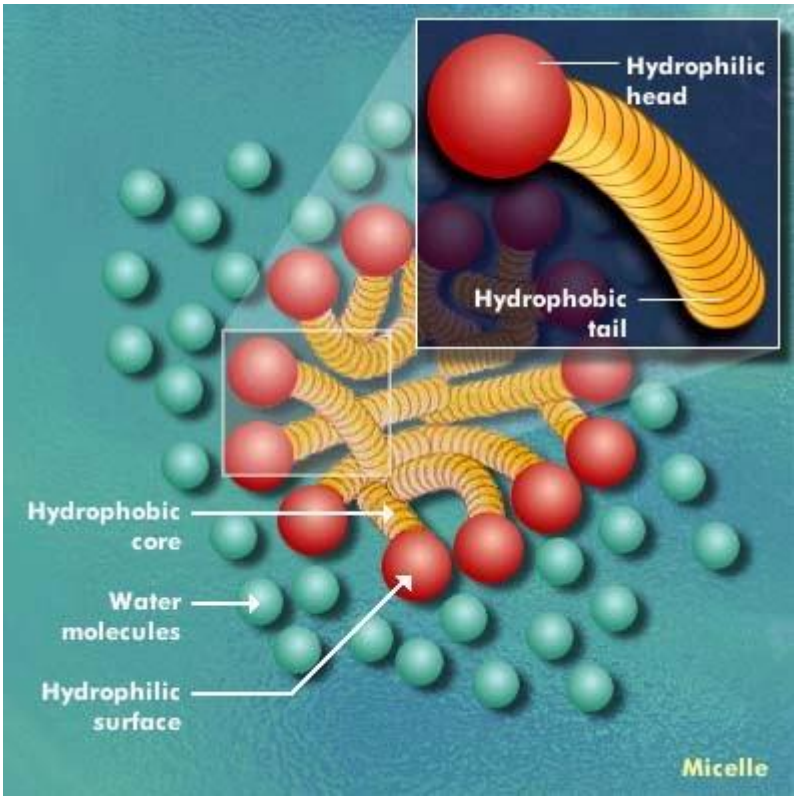

Figure 1-1. The structure of oil-in-water micelles from ref. 13.

1.2.3 Mesoporous silica

MCM-41 [14], the ordered mesoporous silica material that was discovered in 1992, is an appealing candidate in applications such as energy storage, catalyst support, and host material for inclusion compounds, principally because of their high surface area, narrow distributed pore size, and periodic pore channel. Since then, great strides have been made in the creation of a series of mesoporous silicate (i.e. MCM-48, SBA-15 and etcetera) with a vast array of diverse chemical compositions and pore structures [15,16]. In the procedure of synthesis of mesoporous silica, highly mobile surfactants are utilized to generate micelles, and further direct the formation of the porous structures of silica material on the basis of electrostatic or hydrogen-bonding interactions.

Although extensive synthesis approaches and strategies have been employed to fabricate the mesoporous silica material, the mechanic pathway of the formation of MCM-41 structure retains uncertain [17,18]. As shown in Fig. 1-2 [19], the first postulation is that migration and polymerization of silicate anions on the external structures of pre-exist micelles, which result in the formation of the MCM-41 structure; the second postulation is the mutual interaction between the silicate anions and the surfactant cations in aqueous solution ordering the micelles, further leading to the ultimate outcome mesophase. Moreover, mesoporous silica involves porous structure in additional shape, such as hexagonal, cubic, and lamellar, can be formed via controlling the synthesis conditions.

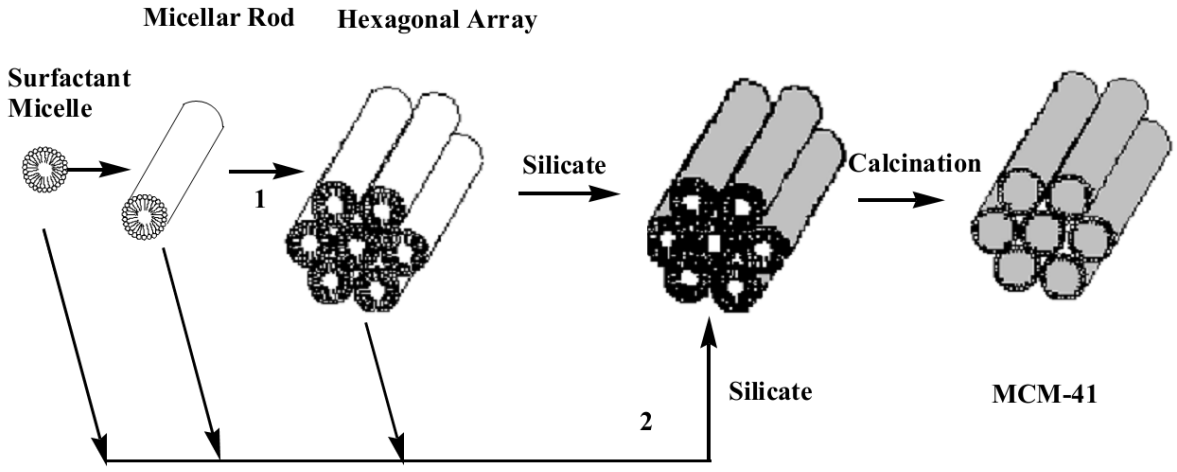

Figure 1-2. Possible mechanistic pathways for the formation of MCM-41 from ref. 19: (1) liquid-crystal phase-initiated and (2) silicate-anion-initiated.

Many novel processes for the introduction of guest nanomaterial to the internal pore channels or external textures of mesoporous silica have provided a platform for the formation of silica nanocomposites with enhanced performance. Several routes to introduce guest molecules to mesoporous silica have been reported, such as 1) co-condensation method; 2) wetness impregnation and ion exchanging; 3) covalent bonding; and 4) surface modification method. The surface modification method (silanization) is utilized to synthesize silica-Au nanocomposites in the thesis.

1.2.4 Chemical etching method and Ostwald ripening

In general, chemical etching is considered as a process of using chemicals (acids, bases or others) to dissolve the unwanted materials such as metals, semiconductors or glass. Ostwald ripening that is first described by Wilhelm Ostwald [20] is an observation of phenomenon associated with the change of an inhomogeneous structure over time in solid solution or liquid sols; in other word, with time increasing, dissolved small crystals or sol particles will redeposit to from larger crystals or sol particles.

In the research of silica, the aim of wet-chemical etching was to dissolve silica by using strong etchant (i.e. HF) [21]. But, recently, it is found that the etching (generated by OH^- ions) of silica initiates the decomposition of silica and generation of silicate; with the time consuming, when the concentration of the silicate reaches the supersaturation, the redeposition of silicate occurs, principally because of energetic favored Ostwald ripening, leading to the reformation of silica. For example, in Fig. 1-3 shows a spontaneous dissolution-regrowth process for the formation of silica hollow structure by using wet-chemical etching [22]. It is found that, the chemical etching of the prior-prepare silica spheres results in a dissolution-regrowth process of silicate, with the ultimate outcome being the formation of hollow silica shell structure. It is known that the etching process of silica generates silicate, and the redepostion of silicate at the surface of the initial silica particles results in the retention of the initial overall shape of silica particles and the formation of hollow silica structures.

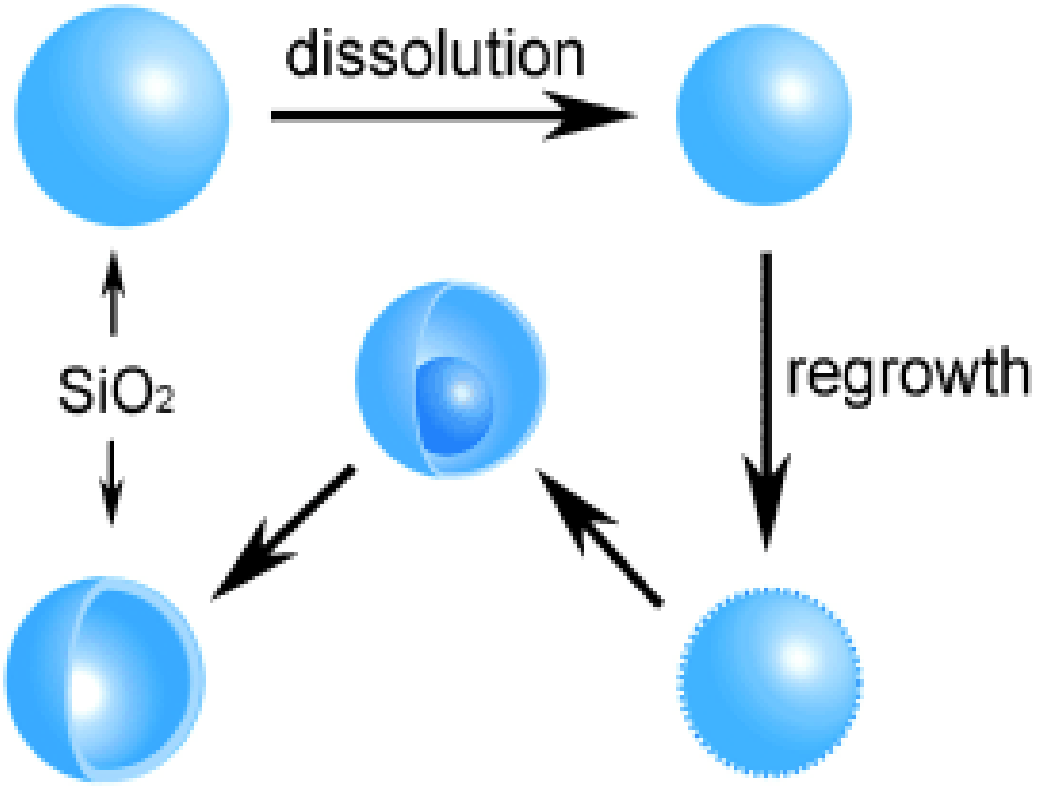

Figure 1-3. Schematic illustration for the formation of hollow silica colloids through a spontaneous dissolution-regrowth process from ref. 22.

1.3 References

[1] Q.J. He, J.L. Shi, J. Mater. Chem. 21 (2011) 5845.

[2] S. Bonacchi, D. Genovese, R. Juris, M. Montalti, L. Prodi, E. Rampazzo, N. Zaccheroni, Angew. Chem. Int. Ed. 50 (2011) 4056.

[3] G.M. Andrés, P.J. Jorge, M.L. Luis, Adv. Mater. 22 (2010) 1182.

[4] M. Roca, A.J. Haes, J. Am. Chem. Soc. 130 (2008) 14273.

[5] Y. Yamada, M. Mizutani, T. Nakamura, K. Yano, Chem. Mater. 22 (2010) 1695.

[6] R.A. Caruso, M. Antonietti, Chem. Mater. 13 (2001) 3272.

[7] F. Caruso, R.A. Caruso, H. MÖhwald, Science 282 (1998) 1111.

[8] Y.D. Yin, R.M. Rioux, C.K. Erdonmez, S. Hughes, G.A. Somorjai, A.P. Alivisatos, Science 304 (2004) 711.

[9] Y.G. Sun, Y.N. Xia, J. Am. Chem. Soc. 126 (2004) 3892.

[10] H.N. Zhang, T.J. Bandosz, D.L. Akins, Chem. Commun. 47 (2011) 7791.

[11] L.L. Hench, J.K. West, Chemical Reviews 90 (1990) 33.

[12] J.M. Seddon, R.H. Templer. Handbook of Biological Physics, Vol. 1, ed. R. Lipowsky, E. Sackmann. (c) 1995, Elsevier Science B.V.

[13] M. Volpert, European Synchrotron Radiation Facility (ESRF), <http://scitech.web.cern.ch/scitech/deeperdown/surfactant.html > (visited 18 September, 2012).

[14] C.T. Kresge, M.E Leonowicz, W.J. Roth, J.C. Vartuli, J.S. Beck, Nature 359 (1992) 710.

[15] V. Alfredsson, M.W. Anderson, Chem. Mater. 8 (1996) 1141.

[16] D. Zhao, J. Feng, Q. Huo, N. Melosh, G.H. Fredrickson, B.F. Chmelka, G.D. Stucky, Science 279 (1998) 548.

[17] N.K. Raman, M.T. Anderson, C.J. Brinker, J. Chem. Mater. 8 (1996) 1682.

[18] A. Sayari, P. Liu, Microporous Mater. 12 (1997) 149.

[19] J.S. Beck , J.C. Vartuli , W.J. Roth , M.E. Leonowicz , C.T. Kresge , K.D. Schmitt , C.T. W. Chu , D.H. Olson , E.W. Sheppard, J. Am. Chem. Soc. 114 (1992) 10834.

[20] W. Ostwald, Lehrbuch der Allgemeiene Chemie, V.1 P. 1 (1896) Leipzig, Germany.

[21] N. Miyata, H. Watanabe, M. Ichikawa, Appl. Phys. Lett. 73 (1998) 3923.

[22] T. Zhang, J. Ge, Y. Hu, Q. Zhang, S. Aloni, Y. Yin, Angew. Chem. Int. Ed. 47 (2008) 5806.

Chapter 2: Materials and characterization

2.1 Materials and methods

2.1.1 Synthesis of silica microspheres

A typical synthesis process was as follow: 50 ml of deionized water and 35 ml ethanol (Decon Labs, Inc., 190 proof) were mixed, and then varied amounts of 1 M sodium hydroxide (Fisher Scientific) were added to adjust the initial synthesis pH. The total volume of the water and ethanol was maintained at 85 ml for a series of predefined water/ethanol ratios; ~0.050 g CTAB (Alfa Aesar, 99+ %) was dissolved in the prepared solvents and the mixture was vigorously stirred until clear; then 12 ml TEOS (Acros Organics, 98%) was slowly added. After reaction, the resultant product was held at room temperature for 3 hours without stirring; the white precipitated was filtered, washed twice with ethanol, and then dried overnight in air at ~60 ºC. Finally, the resultant white powder was calcined for 8 hrs at ~580 ºC to remove any residual CTAB.

2.1.2 Synthesis of ellipsoidal silica nanoparticles

A typical synthesis process was the following: deionized water and ethylene glycol (Sigma-Aldrich, ReagentPlus® ≥ 99%) solution was prepared; CTAB (Alfa Aesar, 99+ %) was dissolved in the prepared solvent; then 1 M ammonium hydroxide (Pharmco Products, Inc.) was added. After slow addition of TEOS (Acros Organics, 98%), the reaction was held at room temperature with stirring. Following the reaction, the white precipitated was filtered, washed with ethyl alcohol (Decon Labs, Inc., 190 proof), then dried overnight in air at ~60 ºC. The final product was calcination for 8 hrs at ~580 ºC to remove any residual CTAB. The molar ratio of

CTAB/NH_4OH/TEOS/ethylene glycol/water was 1:1.2:77.1:381.4:1246.

2.1.3 Synthesis of ellipsoidal silica nanoshells

0.03 g of prior prepared ellipsoidal silica nanoparticles and 0.025 g PVP K29-32 (Acros Organics, M.W. 58,000) were added to a preheated aqueous solvent (50 °C, IKA® ETS-D5) and mixed by mechanical stirring (1,200 rpm) until clear; 0.06 g $NaBH_4$ (Fisher Scientific) was then added to initiate etching, with vigorously stirring for 6 hours. Following the reaction, the silica nanoshells were centrifuged (8,500 rpm) and washed three times with ethyl alcohol. Finally, after drying in air at ~40 ºC overnight, the resultant white powder was collected.

2.2 Characterization

2.2.1 Transmission electron microscopy

Transmission electron microscopy (TEM) is a unique tool in characterization of materials microstructure and crystal structure. Now, the resolution of the acquired TEM images better than 0.1 nm is achievable. The basic setup for TEM is schematically shown in Fig. 2-1 [1].

In a conventional TEM, electrons are emitted from the electron gun and irradiate the specimen through the condenser lens system; the objective lens provides the formation of either images or diffraction pattern of the specimen. The electron intensity distribution behind the specimen is magnified by the stage lens system, converted to digital signals, recorded by a CCD camera, and ultimately presented on screen. As a result, the use of TEM allows us to observe modulations in chemical identity, crystal orientation, and electronic structure of matters on specimen.

In the thesis, the transmission electron microscopy (TEM, Zeiss EM 902) was performed to observe microstructures of silica. A 10 μL aliquot of the silica-alcohol solution was dropped onto a carbon-coated copper grid. After evaporation of the alcohol, the sample was characterized by

TEM at an acceleration voltage of 80 kV.

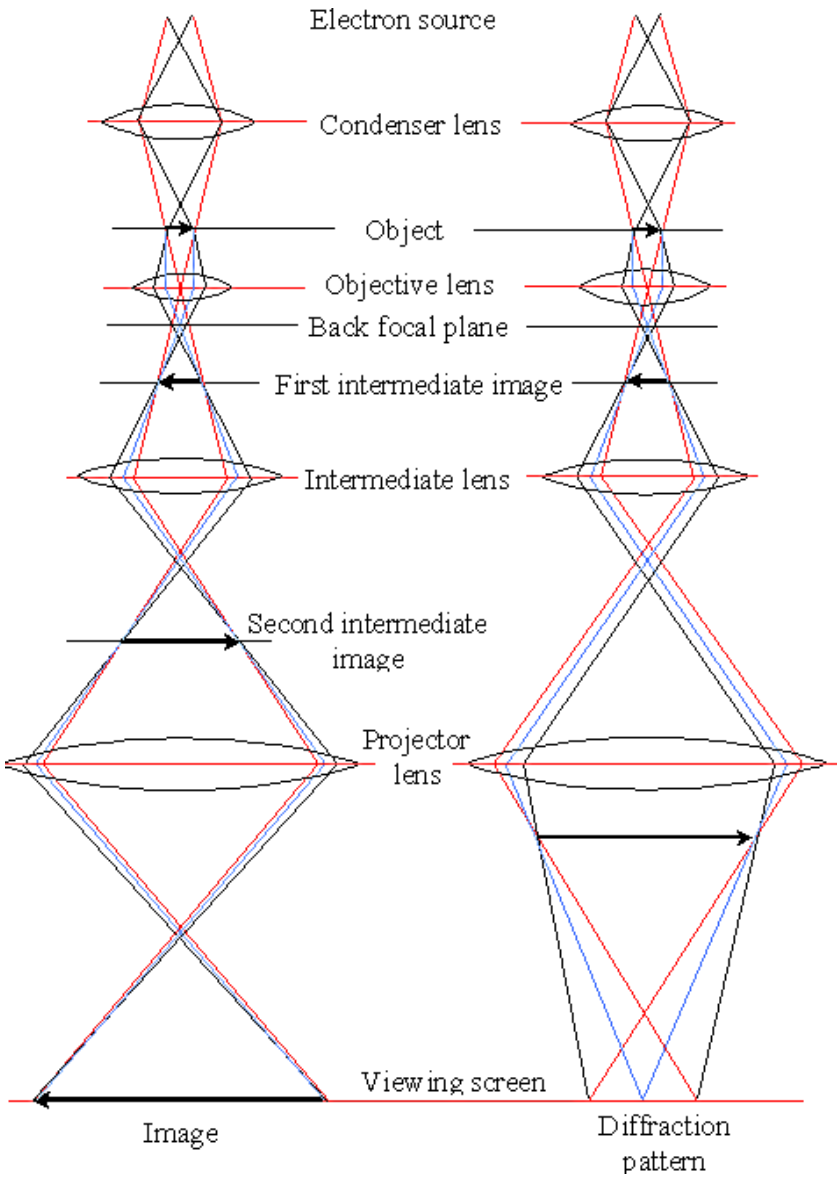

Figure 2-1. Schematic illustration of Transmission Electron Microscope from ref. 1.

2.2.2 Scanning electron microscopy

A scanning electron microscope (SEM) is a tool that characterizes the sample's surface information such as topography and composition by emitting electrons interacting with the atoms that make up the sample producing signals (as indicated in Fig. 2-2 [2]).

Normally, SEM can produce types of signals including secondary electrons, back-scattered electrons (BSE), and characteristic X-rays. The secondary electrons are generated by the interactions of the electron beam with atoms at or near the surface of the sample, and the secondary electron imaging can produce achievable high resolution with less than 1 nm. Back-scattered electrons are formed by the reflection of beam electrons from the sample by elastic scattering. Associated with the use of characteristic X-rays, the componential information on the surface of the sample can be provided by BSE images, principally because of the intensity of the BSE signals strongly relating to the atomic number of the sample. The formation of characteristic X-rays is derived from the occupation of higher-energy electrons on the inner shell electrons of the sample, and the release of energy. The characteristic X-rays are utilized for elemental analysis of the sample.

In the thesis, the same sample preparation for TEM measurement was used for SEM and energy dispersive x-ray spectrometry (EDS) measurements (using a SEM, Zeiss Supra 55 VP). For the SEM analysis, the voltage was 5 kV and the working distance was between 2 and 5 mm. For the EDS analysis, the voltage was 15 kV and working distance was 8.5 mm.

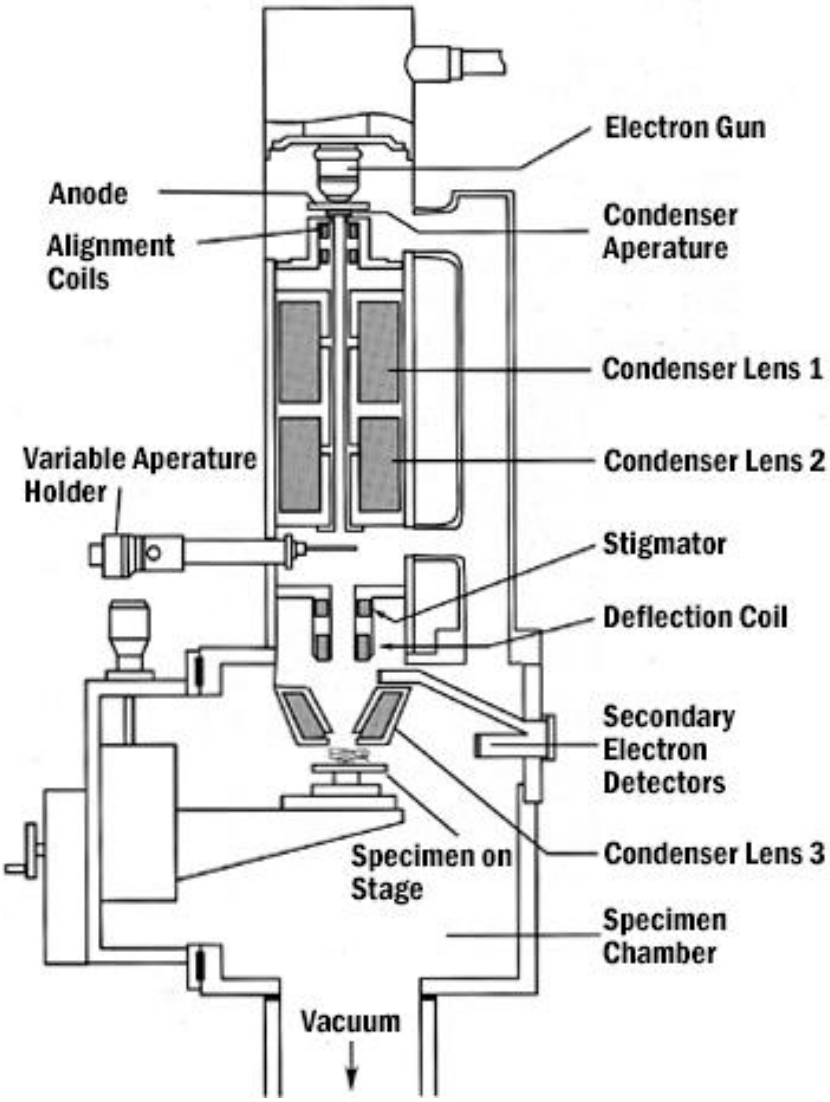

Figure 2-2. Schematic illustration of Scanning Electron Microscope from ref. 2.

2.2.3 X-ray powder diffraction

X-ray powder diffraction is an analytical technique primarily used for revealing the identification of unknown crystalline materials (crystal structures and atomic spacing).

The fundamental principle of X-ray diffraction is largely due to the constructive interference of monochromatic X-rays and a crystalline sample. When Bragg's law is satisfied, the interaction of the incidents X-rays with the sample can generate constructive interference as shown in Fig. 2-3 [3]. By scanning the sample through a range of 2θ angles, due to the random orientation of the powdery sample, all the possibilities of diffraction directions of the lattice can be detected, processed and converted to d-spacings, allowing identifying the sample.

In the thesis, wide angle X-ray powder diffraction measurements were performed to characterize the crystalline structures of silica materials by using a PANalytic X-ray diffractometer in a 2θ range from 10° to 75°; graphite monochromatic CuKα (λ=1.54 Å) radiation was used with a nickel filter.

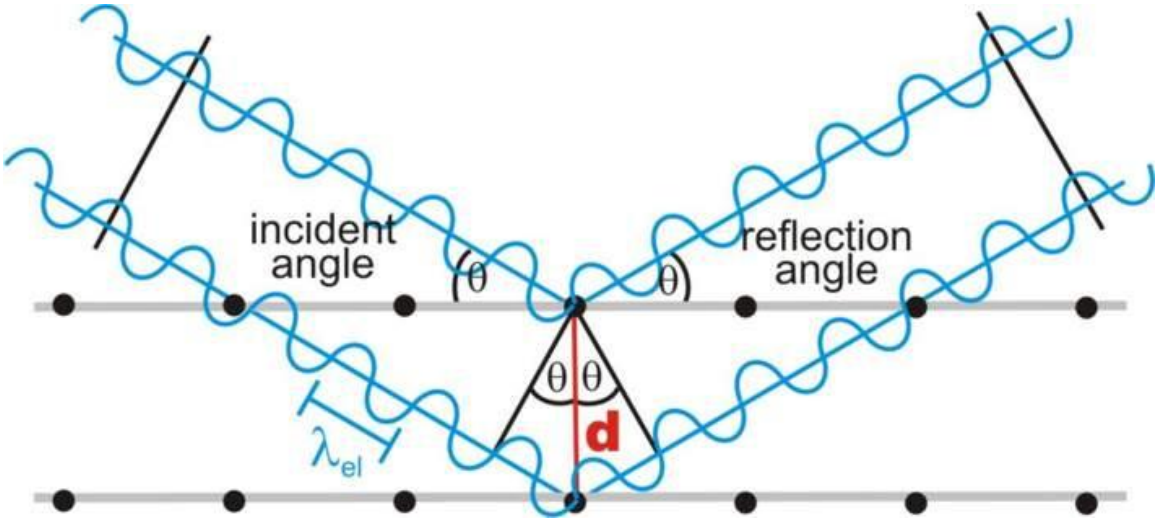

Figure 2-3. Constructive interference of reflected waves ($n\lambda = 2d\sin\theta$) from ref. 3.

2.3 References

[1] D.B. Williams, C.B. Carter, In Transmission Electron Microscopy; Springer US: Boston, MA, (2009) 3-22

[2] The Unviersity of Iowa, <http://www.uiowa.edu/~cmrf/methodology/sem/index.html> (visited 19 September, 2012).

[3] F. Krumeich, Eletron Microscopy ETH Zurich, http://www.microscopy.ethz.ch/bragg.htm (visited 19 September, 2012)

Chapter 3: Synthesis and new structure shaping mechanism of silica particles formed at high pH

3.1 Introduction

Silica materials are appealing candidates in applications such as media for energy storage [1], sensors [2,3], and for drug delivery [4,5], principally because of the vast array of morphologies, derived from the broad spectrum of synthesis approaches [6-10].

It is noted that great strides have been made in synthesis of hollow silica particles. In general, template-assisted approaches have been employed that start with a wide range of starting structures that ultimately result in uniform hollow silica particles [11-13]. But, the advantage of a single-step, facile synthesis approach is generally associated with ease of preparation and separation of useful products. It is well known that synthesis conditions such as solvent compatibility, ease of processability and surface functionality are crucial in determining the morphologies of resultant silica materials. Of course, the size and morphologies of silica products significantly depend on the nature of the solvents [14,15]. In particular, water-ethanol solvents have been shown to lead to the formation of silica particles of a range of spherical morphologies [16,17]. Water-acetone solvents have shown potential to form mesoporous silica nanoparticles [18]. And, recently, in our lab we have utilized water-ethylene glycol solvents to form elliptically shaped silica nanoparticles; surface tension is hypothesized as the driving force in this latter study [19].

Also, the pH of the solvent has been shown to be a crucial factor in synthesis of silica particles. Indeed, emulsion droplets and micellar structures can be controlled when the pH values are

appropriately adjusted, resulting in, for example, hollow and solid silica spheres with porous structure [20,21]. Furthermore, a so-called "pH-induced rapid colloid aggregation" method has been developed to prepare micrometer-sized spheres of mesostructured silica [22]. In this latter case, the variation of pH has resulted in size-controllable mesoporous silica nanoparticles that derived from competition between hydrolysis and condensation of silicon alkoxide [23]. Such materials, because of their permeability and physiological compatibility, have been suggested as potential drug delivery containers, and significantly, controlled release of the encapsulated guest molecules has been effectuated by the change of the pH values [23].

Although much effort has been devoted to control the morphologies of silica materials, results have been somewhat restricted to mild pH synthesis conditions (pH=6~10) since for high pH synthesis the complex, competing processes of hydrolysis and condensation occur [24-26]. However, despite its complexity, the chemical etching technique applied to prior prepared silica particles for the generation of hollow/rattle-type silica structures has received substantial attention [27-33]. It is generally found that the chemical etching of prior-prepared silica particles results in a dissolution-regrowth process of silicate, with the ultimate outcome being the formation of hollow silica shell structures. From such prior studies, although one might conclude that the process of the chemical etching on prior prepared silica particles is well understood much insight into the detailed mechanism might be gained by studying how the morphology of silica materials is affected by carrying out the process under high pH synthesis conditions (pH>12).

We describe, herein, a facile synthesis of solid and hollow silica microspheres via a chemical etching and sol gel process. Briefly, our findings are that the shapes of the silica particles, ranging from uniform solid microspheres to hollow spheres, may be readily controlled by simply

initiating the synthesis using three pH values in three narrow ranges starting at pHs of ~12.3, ~12.8 and ~13.0. In order to more fully assess the steps in the synthesis mechanism for the various initial pHs values, experiments have been conducted using a range of water-ethanol volume ratios (α) and concentrations of CTAB within each range.

3.2 Materials and methods

3.2.1 Materials

Tetraethyl orthosilicate (TEOS; 98%) was obtained from Acros Organics; hexadecyltrimethylammonium bromide (CTAB; >99%) was purchased from Alfa Aesar; ethanol (99.9%) was purchased from Decon Labs, Inc.; methanol from Pharmco Products Inc.; and sodium hydroxide (NaOH) solid was obtained from Mallinckrode Baker, Inc. All reagents were used without further purification. Deionized water was used in all experiments.

3.2.2 Synthesis of silica particles

A typical synthesis process was as follow: 50 ml of deionized water and 35 ml ethanol (99.9%) were mixed, and then varied amounts of sodium hydroxide (1 M) were added to adjust the initial synthesis pH. The total volume of the water and ethanol was maintained at 85 ml for a series of predefined water/ethanol ratios; ~0.050 g CTAB was dissolved in the prepared solvents and the mixture was vigorously stirred until clear; then 12 ml TEOS was slowly added. After reaction, the resultant product was held at room temperature for 3 hours without stirring; the white precipitated was filtered, washed twice with ethanol, and then dried overnight in air at ~60 ºC. Finally, the resultant white powder was calcined for 8 hrs at ~580 ºC to remove any residual CTAB, and represented the final product that was characterized as discussed below.

3.2.3 Characterization

Transmission electron microscopy (TEM, Zeiss EM 902) was performed to observe the size and the morphology of silica particles. To prepare the TEM samples, calcined silica white powders were dispersed in ethanol. A 10 µl aliquot of the silica-ethanol solution was dropped onto a carbon-coated copper grid. After evaporation of the ethanol, the sample was characterized by TEM at an acceleration voltage of 80 kV. The same preparation was used for the scanning electron microscopy and energy dispersive X-ray spectrometry measurements (using a SEM, Zeiss Supra 55 VP). For the SEM analysis, the voltage was 10 kV and the working distance was between 2 to 5 mm. Fourier-transform infrared (FTIR) spectra were obtained in the range of 800-3000 cm^{-1} using a Varian 7000 spectrometer with a resolution of 8 cm^{-1}, and using a MIRacle single horizontal reflection Attenuated Total Reflectance (ATR) accessory. Wide angle X-ray powder diffraction (XRD) measurements were performed using a PANalytic X-ray diffractometer in a 2θ range from 10° to 75°; graphite monochromatic CuKα (λ=1.54 Å) radiation was used with a nickel filter.

3.3. Results and Discussions

3.3.1 The effect of pH on the morphologies of silica materials

For an O/W emulsion system, ammonia hydroxide has been utilized (by others) to catalyze the hydrolysis and condensation of alkoxysilanes; the range of pH values, however, has been somewhat narrow. The use of sodium hydroxide to catalyze hydrolysis and condensation, as we describe herein, allows one to increase the initial pH under which synthesis occurs. Due to chemical etching, higher pH synthesis conditions lead to the decomposition of silica, resulting in the formation of silicates [27]. Moreover, OH^- ions are consumed, facilitating the sol-gel process. In our synthesis, initial pH values were adjusted by addition of selected amounts of sodium

hydroxide (1M) solution, which allows for promotion of sol-gel chemistry and chemical etching at the same time.

Fig. 3-1(a-c) show silica spheres resulting from syntheses at a temperature of 23.5 ºC under different initial pH conditions for reactant concentrations of [CTAB] =1.42mM, [TEOS] = 0.123, and a water/ethanol ratio α =1.428. Fig. 3-1a shows solid spheres are formed at a pH = ~12.3. When the pH of the system was increased to ~12.8 (see Fig. 3-1b), hollow silica spheres with amorphous walls, flacks and bowl-like structures, were obtained; the flacks and bowl-like structures are likely due to partially collapsed gigantic hollow silica spheres (of diameter between 5~10 μm). Furthermore, upon increasing the pH even further to pH= ~13.0 as shown in Fig. 3-1c, uniform microsized solid spheres were again observed to be formed, however this time with remnant flacks.

The effect of lowering the pH value for the reaction system was also investigated. As summarized in Figs. 3-1d and 3-1e, our observations regarding pH change pertain to the morphologies of silica particles for one range versus that for a different range. For example, the micrograph for starting the reaction at pH of ~13.0, after which the reaction had a pH of ~10, was compared with that for which the initial pH was ~12.3 and the final was ~9.0. What was observed, as a result of particle size analysis of the two systems, is that the mean particle sizes were ~831 nm and 807 nm, respectively (see Figs. 3-1d and 3-1e). In these two cases where only solid microspheres were obtained, we deduce that the O/W emulsion particles experienced a modified Stöber synthesis process [34]. We provide in Fig. 3-S1 the time-dependent pH of the systems throughout the reaction; also, Figs. 3-S2 and 3-S3 show the morphologies of silica particles prepared for different initial pH synthesis systems.

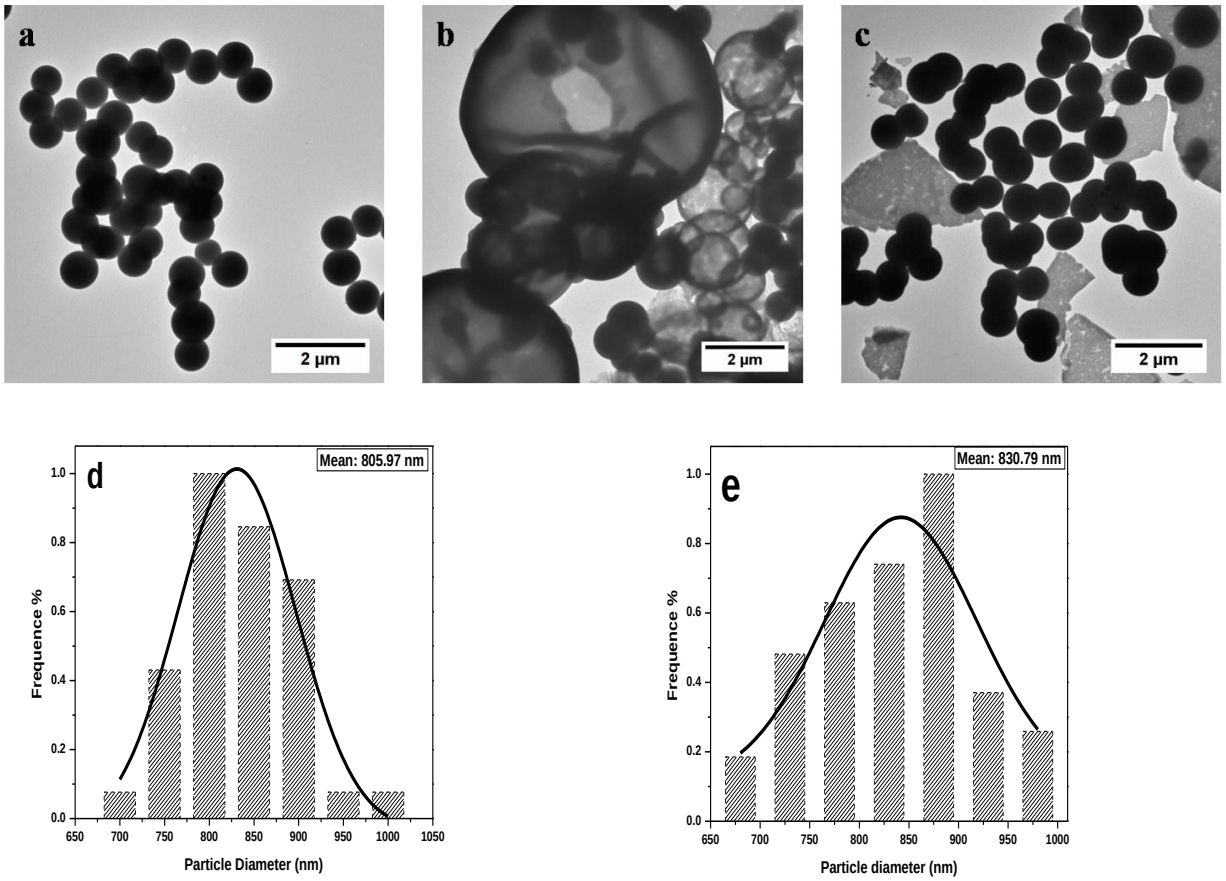

Figure 3-1. (a-c) The TEM images of prepared silica spheres at different pH value: (a) pH = ~12.3, (b) pH = ~12.8 (c) pH = ~13.0. [TEOS] = 0.123, [CTAB] = 1.42mM, α = 1.428. (d-e) particle size analysis of initial pH = ~12.3 and pH = ~13.0 synthesis systems, respectively.

The structural change of silica particles prepared under different synthesis conditions, as mentioned earlier, was further investigated using FTIR-ATR spectroscopy. Absorption bands associated with the C-H bending vibrations were found between 1350 and 1500 cm^{-1} and between 2850 and 3000 cm^{-1} in Fig. 3-2a (open circle curve pertains to hollow sphere sample, while solid line curve pertains to solid sphere sample); it is to be noted that the intense band at ca. 1100 cm^{-1} is attributed to the transverse-optical mode of the Si-O-Si lattice. The presence of C-H bands indicates the existence of nonhydrolyzed OEt groups [35,36]. The absence of identifiable C-H bands in spectra pertaining to solid microspheres (solid-line curve in Fig. 3-2a) suggests that

the TEOS is released to the water phase (and separated from the measured sample) as a result of destruction of the emulsion droplets. It is to be noted that for the TEOS-CTAB-water-ethanol system, the stability of the emulsions resulted from a combination of locally chemical etching and sol-gel formation, and, hence, the presence of nonhydrolyzed TEOS species is good evidence that the emulsions served as templates for formation of hollow silica spheres. FTIR spectra for silica materials prepared at different pHs are shown in Fig. 3-2b and indicate that the asymmetric stretching vibration band for the transverse-optical mode of Si-O-Si experiences a red shift (from 1095 to 1080 cm^{-1}) as a result of the solid-to-hollow morphological conversion [37]. The red shift is attributable to increased bond distance between Si and O atoms, which indicates a greater lattice expansion [38]. The band located at 1190 cm^{-1}, a shoulder peak, is attributable to the longitudinal-optical mode of the Si-O-Si asymmetric bond stretching vibration [37]; the 953 cm^{-1} peak, assignable to Si-OH stretching, is difficult to discern under high pH synthesis conditions (pH>12) shown in Fig. 3-2b, because it overlaps with the strong Si-O-Si asymmetric stretching vibration band.

Additional input into the morphological structures of the samples was obtained using X-ray diffraction (XRD). We ascertained that both the solid and hollow spheres were composed of amorphous substructures (see Fig. 3-S4) [39].

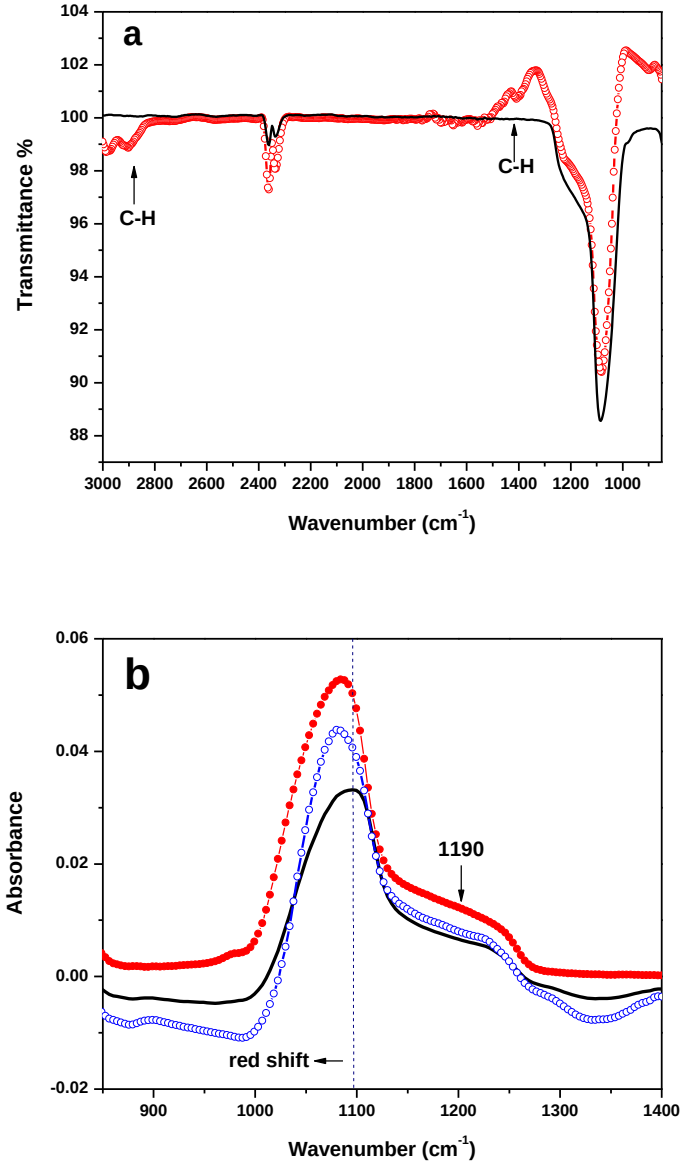

Figure 3-2. (a) FTIR spectra of the hollow and solid silica spheres (open circles: hollow spheres; solid line: solid spheres) (b) FTIR spectra of silica particles prepared with different initial pH (open circles: ~12.8; solid line: ~13.0; filled circles: ~12.3).

3.3.2 The effect of water/ethanol ratio on the morphologies of silica spheres

In our sodium hydroxide catalyzed emulsion system, silica hollow spheres were obtained (see Fig. 3-3a; α = 1.428); but for α = 1.60 uniform spherical silica particles were confirmed (see Fig. 3-3b). On the basis of the reported mechanism, the solubility of the poorly-soluble TEOS species should be increased in the higher ethanol content system (α = 1.428; pH = ~12.7), and solid microspheres should be obtained; while in the lower ethanol content system (α = 1.60; pH = ~12.8), the formation of hollow spheres should be possible. However, the resultant TEM images indicate just the reverse. It is to be inferred that, the occurrence of the strong chemical etching creates surface defects, exposes the internal organic species, and provides pathways for the solvent to enter the emulsion droplets, there through promoting the dissolution of the emulsion. Moreover, water promotes chemical etching, as indicated by the fact that when higher water content was used, no hollow silica structures were obtained (see Fig. 3-S5).

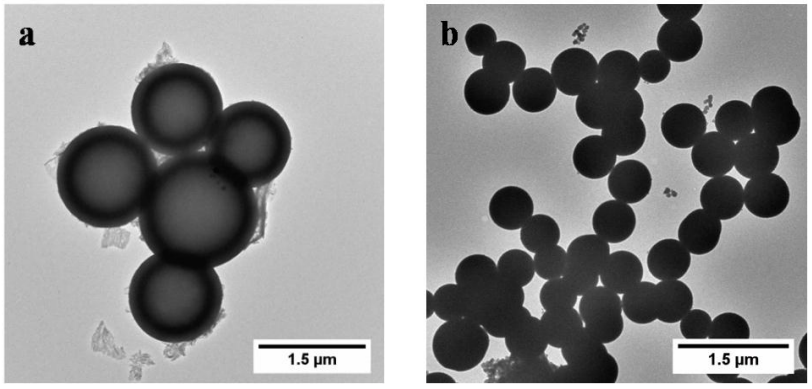

Figure 3-3. The TEM images of prepared hollow spheres at different α: (a) α = 1.428 (b) α = 1.6. [TEOS] = 0.123, [CTAB] = 1.42 mM.

3.3.3 The effect of CTAB on the morphologies of silica spheres

In our emulsion systems, the presence of CTAB resulted in controlled morphologies of the silica particles, with no residual CTAB present after calcination. As shown in Fig. 3-4a, (for which [CTAB] = 1.20 mM), solid silica spheres and network-like structures were formed. Also, upon increasing the CTAB concentration, e.g., to a value of ca. 1.42 mM, only hollow silica spheres were formed as shown in Fig. 3-4b. An explanation for this occurrence is that the positively charged emulsifier (CTAB) at the emulsion interface accelerates the movement of the negatively charged hydrolyzed TEOS, which promotes the sol-gel process [32]. On the other hand, upon increasing [CTAB] to ca. 1.62 mM, uniform solid microspheres were obtained as shown in Fig. 3-4c. We conclude that hydrolysis and condensation of TEOS are both promoted by high concentration of CTAB, while enhancement of the concentration of TEOS promotes miscibility with the water phase, which leads to destruction of the emulsion.

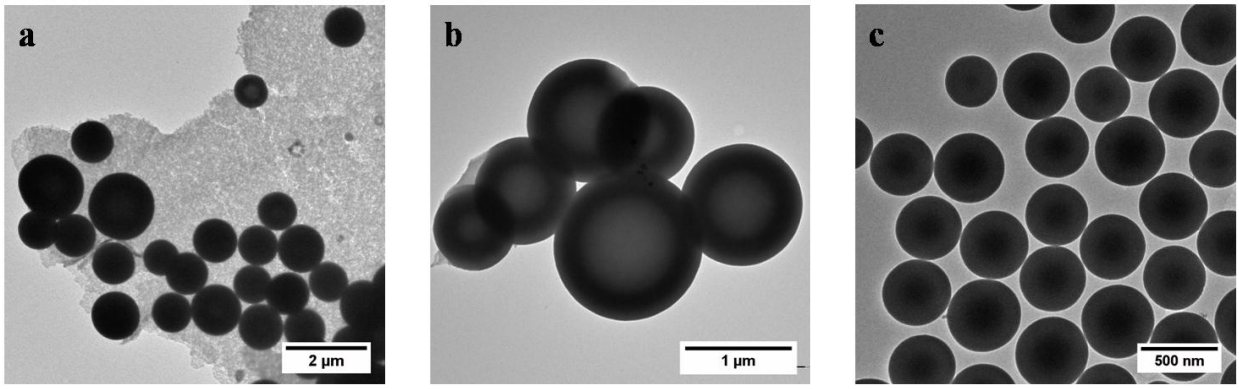

Figure 3-4. The TEM images of prepared hollow spheres with different concentration of CTAB: (a) [CTAB] = 1.20mM, (b) [CTAB] = 1.42mM, (c) [CTAB] = 1.62mM.

3.3.4 Formation mechanism

For ammonia catalyzed water-ethanol systems, prior studies have shown that the morphologies of silica materials is determined by the nonhydrolyzed and partially hydrolyzed TEOS species present [16]. For the NaOH catalyzed water-ethanol-TEOS-CTAB system, the morphologies of silica have been controlled by modifying the synthesis conditions, such as by change of solvents, surfactants, silica precursors, and pH values. However, we have found that the formation of hollow structures is principally defined through retention of the shape of emulsion droplets (see Fig. 3-5). Our studies have suggested that the chemical etching, which, in our case, derives from the presence of OH^- ions, leading to the decomposition of silica. A dissolution-regrowth process and a sol-gel process are put forth to explain how both solid silica as well as hollow silica particles are formed. In Fig. 3-6, the schematic illustration summarizes that the initial values of pH play fundamental roles in determining the morphologies of silica particles: for pH in the lower region, i.e., (~12.3), chemical etching decomposes the silica at the interface of the emulsion droplets, which allows nonhydrolyzed and/or partially hydrolyzed TEOS to flow into the water phase, resulting in the formation of uniform solid microspheres. For the mid pH region that we used, i.e., pH ~ 12.8, the retention of emulsions is facilitated by the both of the efforts of chemical etching and sol-gel process, with hollow silica spheres of a wide distribution resulting. For pH in the high region, i.e., pH ~ 13.0, the strong chemical etching eliminates the emulsions, resulting in silica spheres.

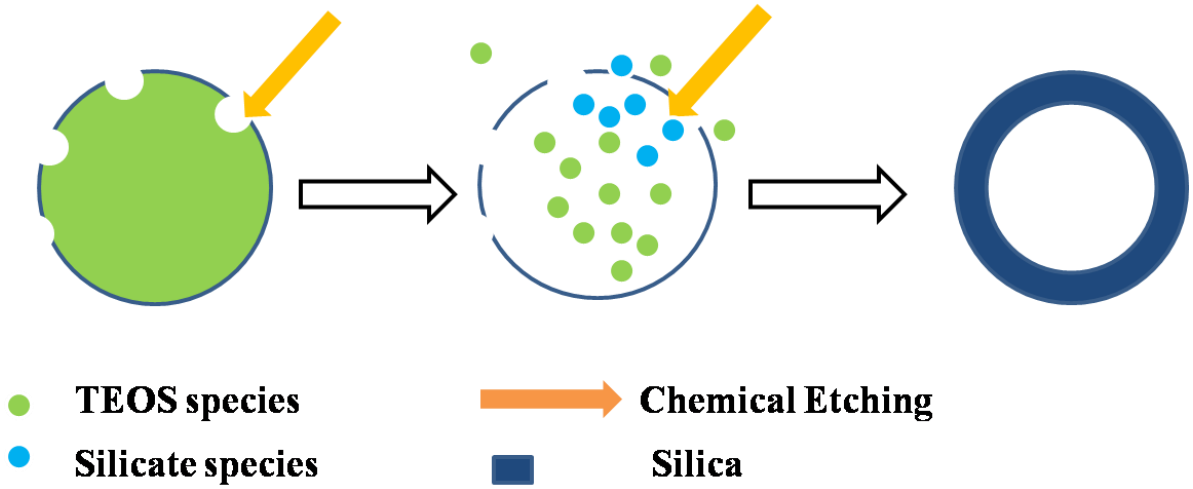

Figure 3-5. Schematic diagrams describing the formation of hollow spheres through "local chemical etching" strategy.

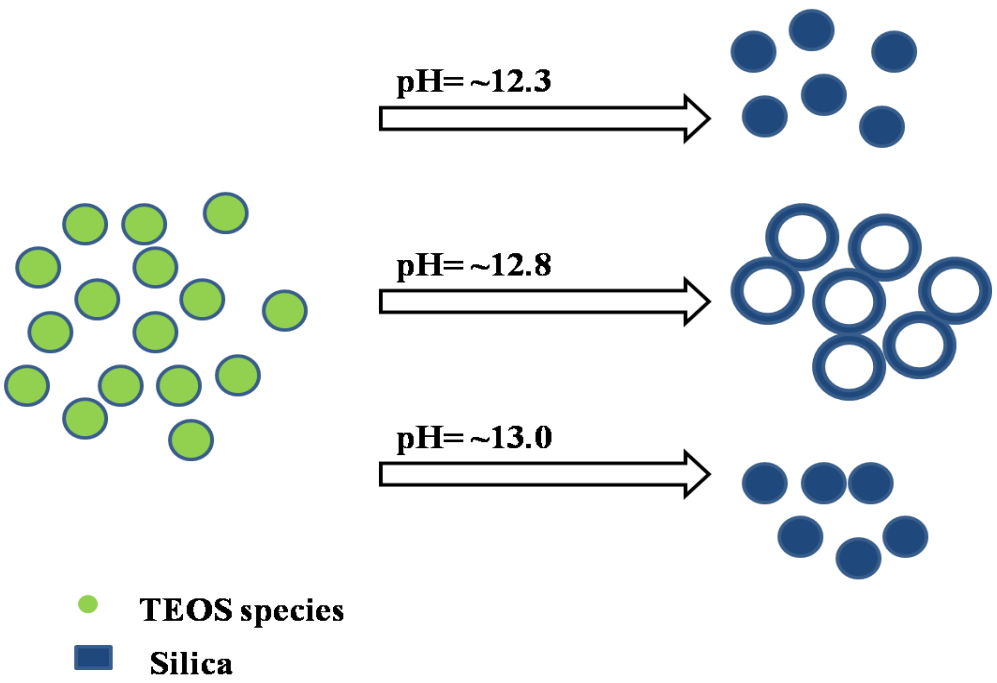

Figure 3-6. Schematic illustration of the morphological control of the silica materials via initial pH values.

3.4. Conclusion

Sodium hydroxide catalyzed synthesis in the water-ethanol-TEOS-CTAB system has been utilized to form uniform solid microspheres and hollow spheres. We have shown the morphologies of the silica materials, such as solid microspheres and hollow spheres, are controlled by adjusting the initial pH values in high region, the water-ethanol volume ratios, and the concentration of CTAB. For the lowest and highest pH synthesis ranges defined herein, different sized solid microspheres are obtained, while for pH between the aforementioned ranges, hollow spheres are formed. The combination of the chemical etching and sol-gel process is put forth to explain the formation of silica materials of a variety of morphologies, and may enable extended academic and commercial utility of silica materials.

3.5 References

[1] Y. Zhao, J.S. Zhang, D.L. Akins, J.W. Lee, Industrial & Engineering Chemistry Research, 50 (2011) 10024.

[2] S. Bonacchi, D. Genovese, R. Juris, M. Montalti, L. Prodi, E. Rampazzo, N. Zaccheroni, Angew. Chem. Int. Ed. 50 (2011) 4056.

[3] M. Roca, A.J. Haes, J. Am. Chem. Soc. 130 (2008) 14273.

[4] Q. He, J.L. Shi, J. Mater. Chem. 21 (2011) 5845.

[5] Y.H. Jin, A. Li, S.G. Hazelton, S. Liang, C.L. John, P.D. Selid, D.T. Pierce, J.X. Zhao, Coordination Chemistry Reviews, 253 (2009) 2998.

[6] F. Caruso, R.A. Caruso, H. MÖhwald, Science 282 (1998) 1111.

[7] Y.D. Yin, R.M. Rioux, C.K. Erdonmez, S. Hughes, G.A. Somorjai, A.P. Alivisatos, Science 304 (2004) 711.

[8] Y.G. Xia, Y.N. Xia, J. Am. Chem. Soc. 126 (2004) 3892.

[9] M.H. Yu, H.N. Wang, X.F. Zhou, P. Yuan, C.Z. Yu, J. Am. Chem. Soc. 129 (2007) 14576.

[10] J.G. Wang, F. Li, H.J. Zhou, P.C. Sun, D.T. Ding, T.H. Chen, Chem. Mater. 21 (2009) 612.

[11] Q.B. Wang, L. Yan, H. Yan, Chem. Commun. (2007) 2339.

[12] L. Zhang, M. D'Acunzi, M. Kappl, G.K. Auernhammer, D. Vollmer, C.M. van Kats, A. van Blaaderen, Langmuir 25 (2009) 2711.

[13] X.W. Lou, L.A. Archer, Z.C. Yang, Adv. Mater. 20 (2008) 1.

[14] W.C. Yoo, A. Stein, Chem. Mater. 23 (2011) 1761.

[15] Y. Yamada, K. Yano, Micropor. Mesopor. Mater. 93 (2006) 190.

[16] H.J. Zhang, J. Wu, L.P. Zhou, D.Y, Zhang, L.M. Qi, Langmuir 23 (2007) 1107.

[17] Z.G. Teng, Y.D. Han, J. Li, F. Yan, W.S. Yang, Micropor. Mesopor. Mater. 127 (2010) 67.

[18] J.C. Zhang, M. Liu, A.F. Zhang, K.F. Lin, C.S. Song, X.W. Guo, Solid State Sci. 12 (2010) 267.

[19] H.N. Zhang, T.J. Bandosz, D.L. Akins, Chem. Commun. 47 (2011) 7791.

[20] H.N. Zhang, Y. Zhou, Y.R. Li, T.J. Bandosz, D.L. Akins, J. Colloid Interface Sci. 375 (2012) 106.

[21] Z.G. Feng, Y.S. Li, D.S. Niu, L. Li, W.R. Zhao, H.R. Chen, L. Li, J.H. Gao, M.L. Ruan, J.L. Shi, Chem. Commun. (2008) 2629.

[22] L.M. Yang, Y.J. Wang, G.S. Luo, Y.Y. Dai, Micropor. Mesopor. Mater. 94 (2006) 269.

[23] Z.A. Qiao, L. Zhang, M.Y. Guo, Y.L. Liu, Q.S. Huo, Chem. Mater. 21 (2009) 3823.

[24] L.L. Hench, J.K. West, Chem. Rev. 90 (1990) 33.

[25] C.J. Brinker, Journal of Non-Crystalline Solids 100 (1988) 31.

[26] S.L. Chen, P. Dong,G.H. Yang, J.J. Yang, Ind. Eng. Chem. Res. 35 (1996) 4487.

[27] T.R. Zhang, J.P. Ge, Y.X. Hu, Q. Zhang, S. Aloni, Y.D. Yin, Angew. Chem. Int. Ed. 47, (2008) 5806.

[28] T.R. Zhang, Q. Zhang, J.P. Ge, J. Goebl, M.W. Sun, Y.S. Yan, Y.S. Liu, C.L. Chang, J.H. Guo, Y.D. Yin J. Phys. Chem. C 113 (2009) 3168.

[29] Q. Zhang, T.R. Zhang, J.P. Ge and Y.D. Yin, Nano Lett. 8 (2008) 2867.

[30] Y. Chen, H.G. Chen, L.M. Guo, Q.J. He, F. Chen, J. Zhou, J.W. Feng, J.L. Shi, ACS Nano 4 (2010) 529.

[31] X. Du, J.H. He, ACS Appl. Mater. Interfaces 3 (2011) 1269.

[32] X.L. Fang, C. Chen, Z H. Liu, P.X. Liu, N.F. Zheng, Nanoscale 3 (2011) 1632.

[33] T. Asefa, Y.J. Shi, J. Mater. Chem. 18 (2008) 5604.

[34] W. Stöber, A. Fink, E. J. Bohn, J. Colloid Interface Sci. 26 (1968) 62.

[35] D.S. Jacob, A. Gedanken, J. Am. Ceram. Soc. 91 (2008) 3024.

[36] J.L. Koenig, Acc. Chem. Res. 14 (1981) 171.

[37] S. Bruynooghe, F. Bertin, A. Chabli, J.C. Gay, B. Blanchard, M. Couchaud, Thin Solid Films 313 (1998) 722.

[38] H. Zhu, Y.G. Ma, Y.G. Fan, J.C. Shen, Thin Solid Films 397 (2001) 95.

[39] V. Bansal, A. Ahmad, M. Sastry, J. Am. Chem. Soc. 128 (2006) 14059.

[40] Z. Lin, J.J. Cai, L.E. Scriven, H.T. Davis, J. Phys. Chem. 98 (1994) 5984.

[41] A. López-Noriega, E. Ruiz-Hernandez, S.M. Stevens, D. Arcos, M.W. Anderson, O. Terasaki, M. Vallet-Regí, Chem. Mater. 21 (2009) 18.

3.6 Supplementary information

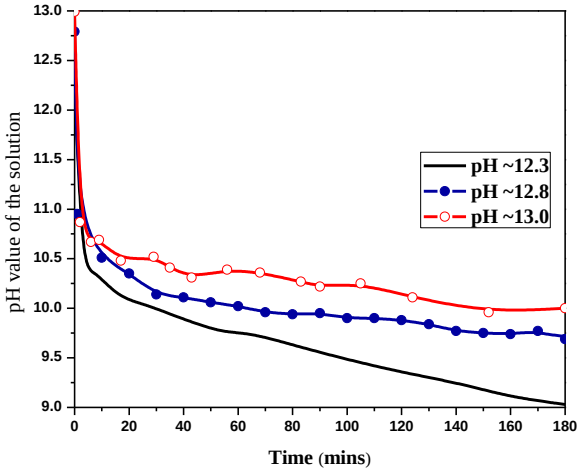

Figure 3-S1. The measurement of pH values of water-ethanol-CTAB-TEOS systems with time-dependent (solid lines: ~12.3; filled circles: ~12.8; open circles: ~13).

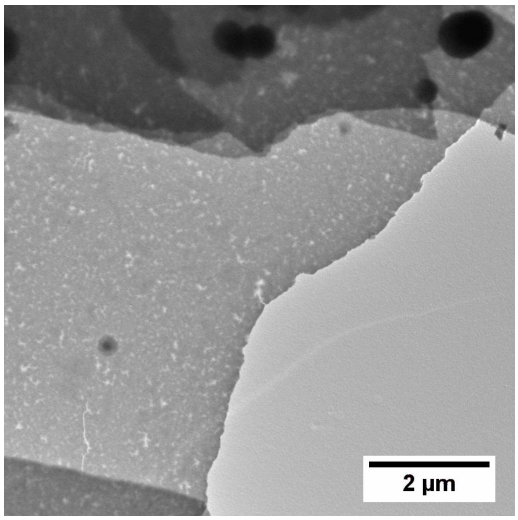

Figure 3-S2. The TEM images of network-like structure with initial pH = ~12.45 [TEOS] = 0.123, [CTAB] = 1.42mM, µ = 1.428.

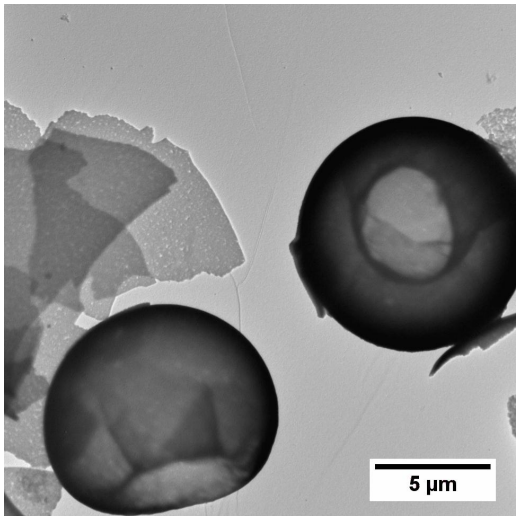

Figure 3-S3. The TEM images of gigantic bowl-like structure with initial pH = ~12.7 [TEOS] = 0.123, [CTAB] = 1.42mM, µ = 1.428.

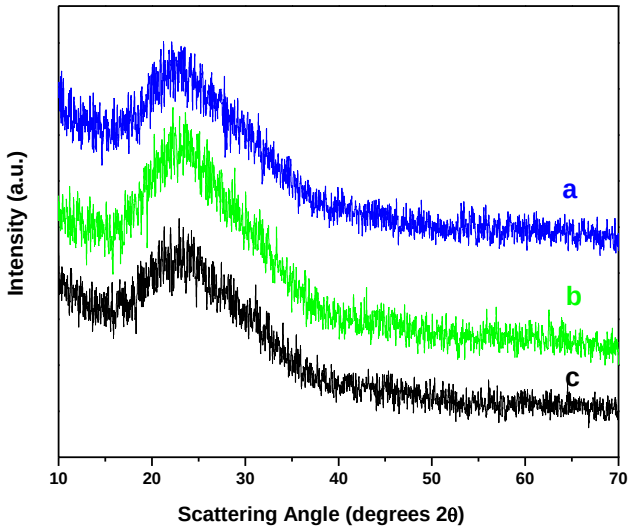

Figure 3-S4. XRD patterns of the silica materials obtained under different initial pH values: (a) pH = ~12.3; (b) pH = ~12.8; (c) pH = ~13.0.

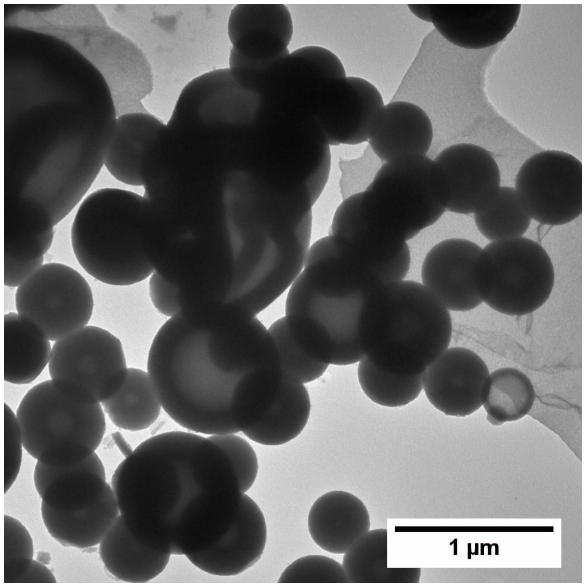

Figure 3-S5. The TEM image of prepared hollow silica spheres with water-methanol-CTAB-TEOS emulsion system ([TEOS] = 0.095, [CTAB] = 1.42mM, α =1.428).

Chapter 4: Template-free synthesis of silica ellipsoids

4.1 Introduction

For template-assisted syntheses of silica nanostructures, the ultimate overall shapes of silica materials are in large measure determined by the templates [1,2]. As a result, a variety of morphologies and compositions of silica materials have been achieved, and, in particular, silica nanohybrids have been developed, and represent appealing candidates in applications such as hydrogen storage, catalysis, and drug delivery [3-6]. However, a facile, template-free synthesis approach would possess several advantages, including ease of preparation and possibly elimination of the need for a scaffold structure altogether.

As has been found by researchers, solvents play a crucial role, in a template free approach, in determining the overall morphologies and compositions of resultant silica materials. As examples, the Stöber [7] and "modified Stöber" [8-10] methods use a water/ethanol reaction system to control the diameters of spherical silica particles and to prepare ordered mesoporous silica spheres, respectively. Additionally, silica nanoparticles have been converted from solid spherical to hollow spherical structures by varying ratios of water to ethanol [11]. In addition to the water/ethanol system, morphologically controllable mesoporous silica nanoparticles have been synthesized using water/acetone solvents [12]. Also, water/methanol, ethylene glycol, polyethylene glycol, glycerine, and poly(vinyl alcohol) (PVP) have been utilized to modify the size of porous spherical silica particles [13]. It is to be noted that, despite the fact that extensive efforts have been made to modify the morphology of silica materials with different solvents, the vast majority of reported literature point to the formation of silica structures that are either spherical-hollow, mesoporous, or solid. As a result, it would appear clear that self-assembled

spherical shapes are generally favored and would likely occur for any homogeneous synthesis process. Moreover, the formation of silica materials with non-spherical morphologies is generally made possible through utilization of non-symmetrical templates [14,15]. As examples of this latter fact, we note that α-Fe_2O_3 spindles have been used as templates to fabricate silica ellipsoids. Specifically, Lou et al. [16] have coated α-Fe_2O_3 spindles with silica to form structured materials that are classified as non-spherical rattles. Also, Zhang et al. [17] have converted ellipsoidal α-Fe_2O_3/SiO_2 core-shell particles into yolk-shell structures through a chemical etching approach. Furthermore, Au-induced PVP aggregates have been described by Zhang et al. [18] to form anisotropic silica nanostructures, and Anke et al. [19] have developed this method to synthesize monodispersed rodlike silica colloids with PVP as templates. However, the complexity of the preparation and the presence of non-removable solid cores have resulted in limited utility for the resultant silica non-spherical structures.

4.2 Materials and methods

4.2.1 Materials

Tetraethyl orthosilicate (TEOS, 98%) was obtained from Acros Organics; hexadecyltrimethylammonium bromide (CTAB, 99+ %) was purchased from Alfa Aesar; ethylene glycol, ReagentPlus ® (≥99%) was purchased from Sigma-Aldrich; Ammonium hydroxide (NH_4OH) was purchased from Pharmco products, Inc.; and ethyl alcohol 190 proof was obtained from Decon Labs, Inc. All reagents were used without further purification. Deionized water was used in all experiments.

4.2.2 Synthesis of silica ellipsoids

A typical synthesis process was as follow: 50 mL of deionized water and 35 mL ethylene glycol

(≥99%) were mixed; ~0.2525 g CTAB was dissolved in the prepared solvents and the mixture was vigorously stirred until clear; and then 0.842 mL ammonium hydroxide (1 M) was added. The total volume of the water and ethylene glycol was maintained at 85 ml for a series of predefined ratios. After 12 mL TEOS was slowly introduced, the reaction was held at room temperature with stirring. Following the reaction, the white precipitated was filtered, washed with 500 mL ethyl alcohol, and then dried overnight in air at ~60 ºC. Finally, the resultant white powder was calcination for 8 hrs at ~580 ºC to remove any residual CTAB, and represented the final product that was characterized as discussed below. The molar ratio of CTAB/NH_4OH/TEOS/ethylene glycol/water was 1:1.20:77.14:897.14:3968.57, when 50 mL water and 35 mL ethylene glycol were applied.

4.2.3 Characterization

Transmission electron microscopy (TEM, Zeiss EM 902 and JOEL JEM-2100) was performed to observe the size and the morphology of silica particles. To prepare the TEM samples, calcined silica white powders were dispersed in ethanol. A 10 µl aliquot of the silica-ethanol solution was dropped onto a carbon-coated copper grid. After evaporation of the ethanol, the sample was characterized by TEM at acceleration voltages of 80 and 200 kV, respectively.

The same preparation as above was used for the scanning electron microscopy measurements (using a SEM, Zeiss Supra 55 VP). For the SEM analysis, the voltage was 10 kV and the working distance was between 2 to 5 mm.

Fourier-transform infrared (FTIR) spectra were obtained in the range of 800-5000 cm^{-1} using a Varian 7000 spectrometer with a resolution of 2 cm^{-1}, and using a MIRacle single horizontal reflection Attenuated Total Reflectance (ATR) accessory.

Wide angle X-ray powder diffraction (XRD) measurements were performed using a PANalytic X-ray diffractometer in a 2θ range from 1° to 10°; graphite monochromatic CuKα (λ=1.54 Å) radiation was used with a nickel filter.

Nitrogen adsorption isotherms were measured using an ASAP 2010 analyzer (Micromeritics, Norcross, GA, USA) at -196 ^{o}C. Before the experiment, the samples were degassed at 120 °C to a constant pressure of 10^{-4} Torr. The isotherms were used to calculate the specific surface area, S_{BET}; micropore volume, V_{mic}; total pore volume, V_t; and pore size distribution. The micropore volume was calculated using Dubinin-Astakhov approach and the total pore volume seen by the nitrogen molecules, from the last point of the isotherms based on the volume of nitrogen adsorbed; the volume of mesopores, Vmes, represents the difference between those two values. The relative microporosity was calculated as the ratio of the micropore volume to the total pore volume. Pore size distributions (PSDs) were determined using Barrett-Joyner-Halenda (BJH) method.

4.3 Results and discussions

We describe a simple approach, without the need for non-symmetrical templates, that uses water and ethylene glycol (EG) as the water/oil (w/o) ingredients to create self-assembled silica structures in a w/o system, where the reaction predominantly occurs at the w/o interface. More specifically, we have observed that if fresh TEOS is introduced into an ammonia catalyzed reaction system, hydrolysis and polymerization occur, which generate silica nuclei. And, upon using appropriate volume ratios of water and EG, proper amounts of TEOS and ammonia, as well as a suitable concentration of CTAB, anisotropic surface tensions at the interface are found to be exerted on the nuclei during the sol-gel process. We hypothesize that anisotropic surface tension forces (γ_{po}, γ_{pw}, γ_{ow}) influence the nucleation process and lead to the formation of the

nonspherically shaped silica.

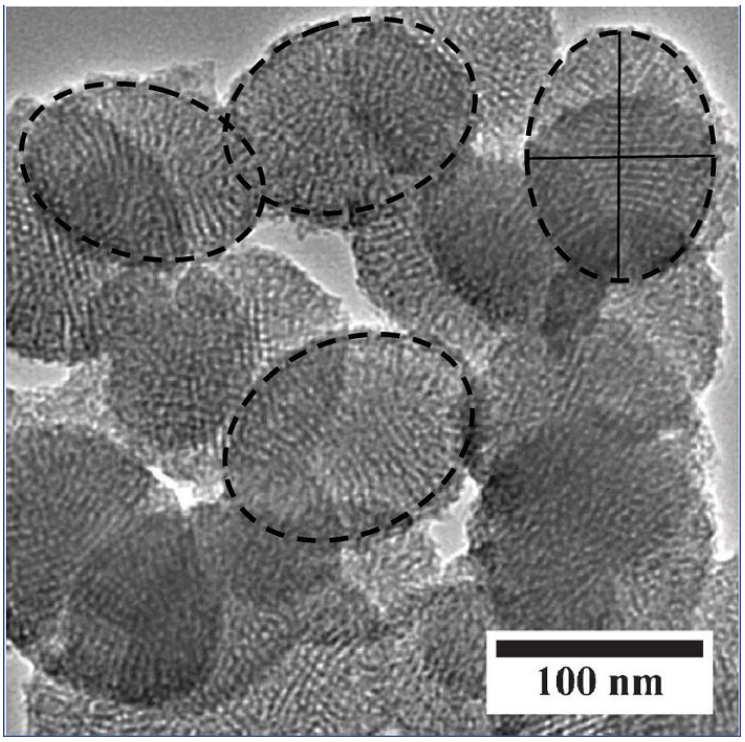

Figure 4-1. TEM image of mesoporous ellipsoidal silica.

In order to test our hypothesis, a number of experiments have been conducted. For example, different volume ratios of water to EG (α) were studied, while the other parameters (the amount of TEOS, ammonia, CTAB, temperature, and reaction duration) were held constant. As shown in Fig. 1, the silica particles were elliptical (dashed curve) and the aspect ratio was approximately 4:3. It is inferred that when a volume ratio (α = 1.43; which we term as "high" for our studies) was used, uniform and monodispersed silica ellipsoids are obtained. The pore size is found to be ca. 3 nm.

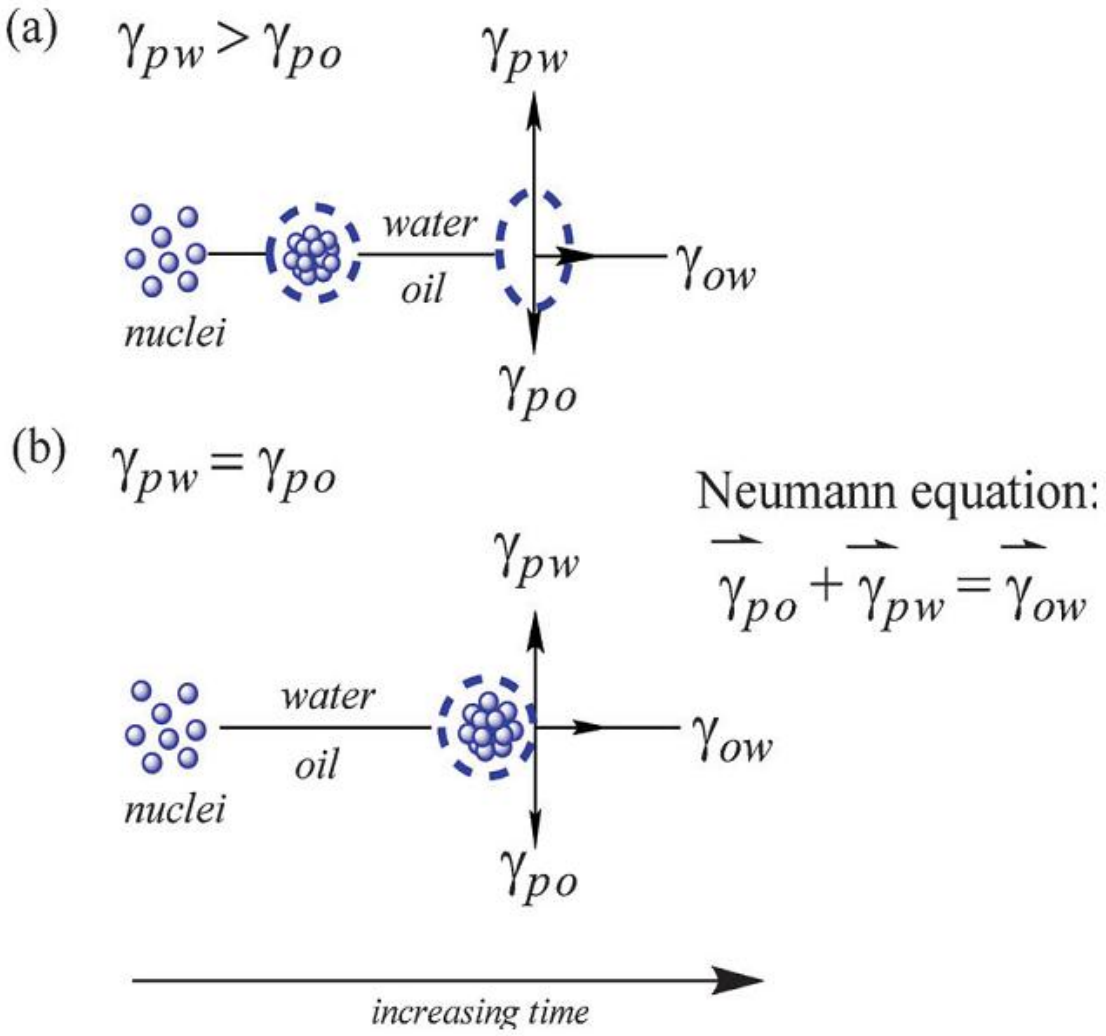

Scheme 4-1. Schematic illustration of the formation of a) ellipsoidal silica and b) spherical silica.

Our explanation of this occurrence is provided in the scheme shown in Sch. 4-1a, which is reminiscent of formation of asymmetric colloidal particles at an oil-water interface. The diagram provides a mechanism showing silica nuclei coalescing and forming self-assembled clusters (enclosed in a dashed circle). As the reaction proceeds, the diagram incorporates the concept that an imbalance in surface tension at the w/o interface leads to an elongation of the nascent particle in the water phase relative to its dimension in the oil phase. The reasoning in support of this supposition is that when $\gamma_{pw} > \gamma_{po}$, a shape transformation (from essentially a circular particle cluster) can be anticipated to be associated with the asymmetric pull on the particles in a direction perpendicular to the w/o interface. Moreover, since the condensed silica particle is hydrophilic, it is to be further anticipated that as time progresses, an even larger water phase surface force would occur ($\gamma_{pw} >> \gamma_{po}$), since the surface area of the silica particles would be increasing with time, resulting in an increase in the growth in the water phase, and hence an elongation perpendicular to the interface: i.e., the nuclei would become ellipsoidal in shape, instead of spherical.

The same model as described above explains the condition necessary for the formation of spherical particles. Specifically, we have found that when the w/o volume ratio has values less than 1, which we characterize for discussion purposes as being "low," we infer that the surface tensions in both the water and oil phases are essentially equal, i.e., $\gamma_{pw} = \gamma_{po}$. (Note: we have expressly studied systems with α = 0.89 and 0.55). For this case, where w/o is less than 1, as depicted in Sch. 4-1b, the two liquids are miscible and there is no net pull on the shape in any direction, hence the resultant shape is spherical. As indicated in Sch. 4-1a and 4-1b, the concepts presented here are consistent with Neumann's equation-of-state, which deals with equilibrium interfacial surface tension on silica nuclei [20-22]. It is to be noted that Young's equation would

not apply to our system since the size of the nuclei is much smaller than one micron, as is implicit in Young's model [23].

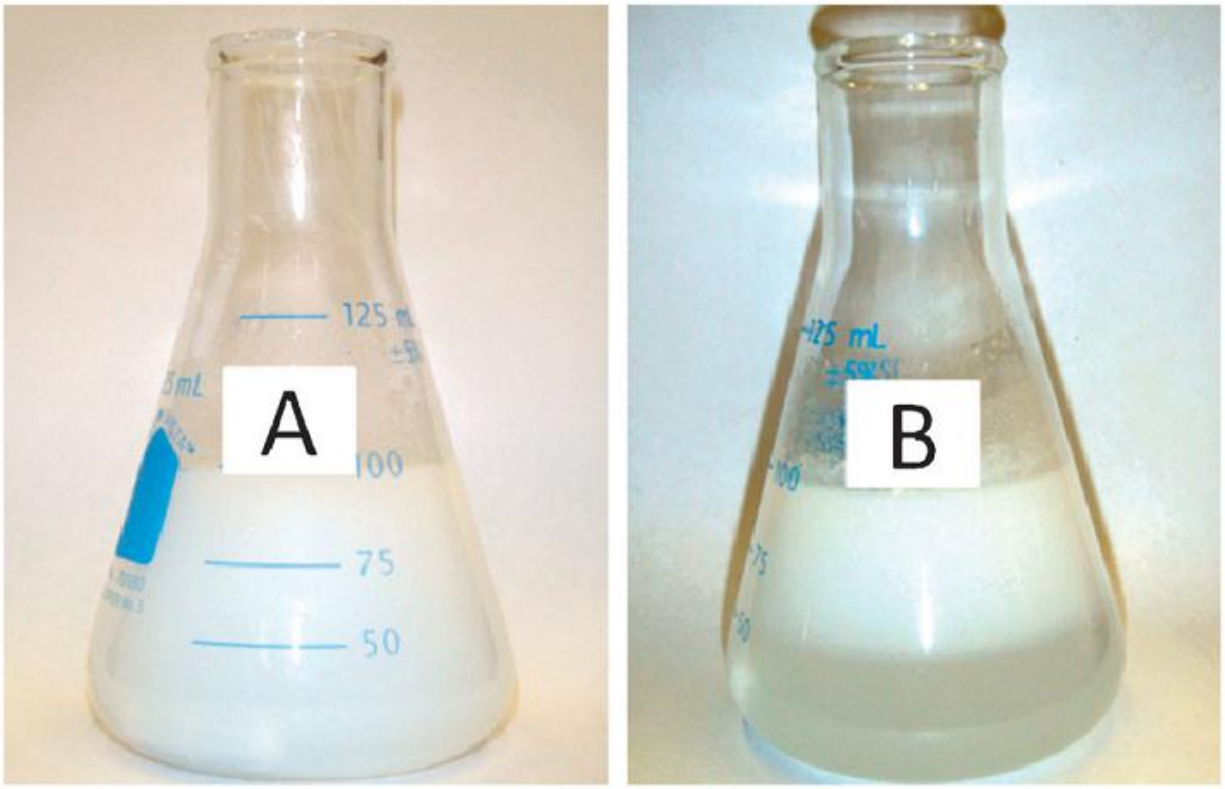

Figure 4-2. Observations of different volume ratio systems: (a) $\alpha = 0.55$; (b) $\alpha = 1.43$.

To test the mechanism that we propose, a range of α values, with a fixed quantity of CTAB, was used in a number of reactions, and resultant structural characteristics were assessed [24]. For a low volume ratio ($\alpha = 0.55$), silica particles were found to be dispersed throughout a stable w/o mixture (see Fig. 4-2a). As mentioned earlier, we deduce that the w/o phases, for such a system, should possess essentially equal surface tensions ($\gamma_{pw} = \gamma_{po}$), and should lead to spherical silica, which is indeed the case. For the high volume ratio system ($\alpha = 1.43$), on the other hand, which leads to the formation of two immiscible phases immediately, we find that the synthesized silica particles ultimately find themselves suspended in the upper water phase, leaving the relatively

clear oil phase at the bottom (see Fig. 4-2b). It is to be noted that the quantity of water used was a significant factor in the rate of reaction and the size of silica particles formed; i.e., for high ratio system, more water was used, which resulted in the sol-gel process occurring more rapidly. From the direct observation of the phase separation, the miscibility of w/o phases is obvious, and is likely quite important in influencing shapes of silica particles that form. It is reasonable to deduce that anisotropic surface tensions, for our system, are exerted and lead to formation of silica ellipsoids.

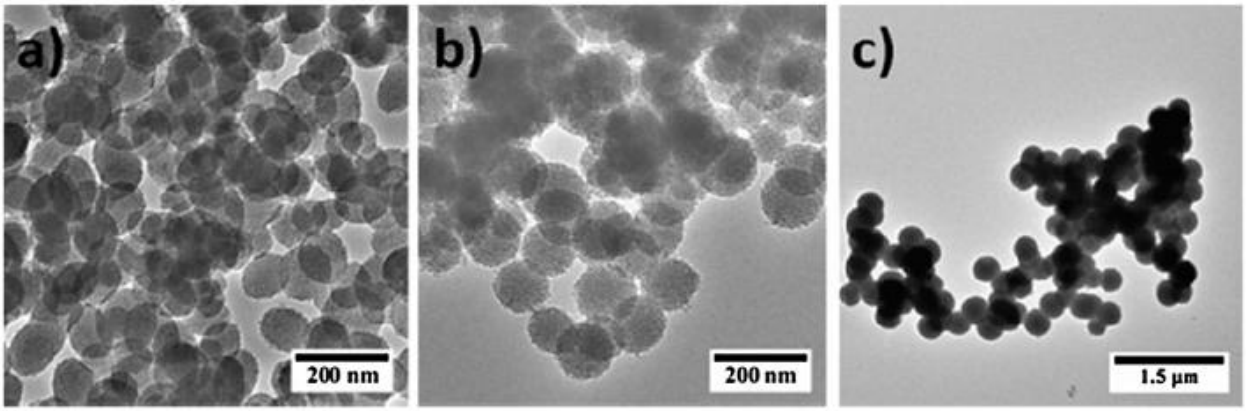

Figure 4-3. TEM images of silica nanoparticles synthesized with different volume ratios of water to ethylene glycol: (a) $\alpha = 1.43$, (b) $\alpha = 0.89$ and (c) $\alpha = 0.55$.

Transmission electron microscopy (TEM) measurements have played a key role in allowing us to formulate the mechanism that is proposed herein. As a prime example, Fig. 4-3a reveals that ellipsoidal silica nanoparticles are observed upon conducting synthesis with a high volume ratio ($\alpha = 1.43$). We note that the average long axis dimension of the silica ellipsoids is approximately 111 nm, and the aspect ratio is about 4:3. Upon making $\alpha = 0.89$, but keeping other conditions the same, uniform mesoporous spherical silica were obtained as shown in Fig. 4-3b. In this latter case, the average diameter estimated from the image was approximately 124 nm. Furthermore, upon decreasing the volume ratio to $\alpha = 0.55$, a tremendous increase in diameters of spherical

silica particles occurs as shown in Fig. 4-3c, where the diameter increased to ca. 375 nm. While, in samples with α = 0.89 and 0.55, ellipsoidal particles were found. From our TEM observation, we observe that different volume ratios play an essential role in defining the ultimate morphology of silica particles. We also observed, through more detailed analysis of the TEMs, that a range of particles are formed with decreasing α [25].

The porosity parameters for our silica particles, acquired from nitrogen adsorption isotherms are shown in Table 4-1. The silica particles that are synthesized with α = 0.55 are found to have the larger pore volume (V_t) as well as larger micropore volume (V_{mic}). This is the natural consequence of packing particles that differ in sizes. The nitrogen isotherm measured for the silica ellipsoids (α = 1.43) have a different shape than those of the other two samples, as shown in Fig. 4-S5; we find that even though the size of the silica particles (for α = 1.43) is the smallest of the three, their ellipsoidal shape affect their packing arrangement resulting in a larger void space/pore volume ratio. As a result of this observation, the silica particles would be classified as micro/mesoporous.

Table 4-1. Porosity of silica products determined from nitrogen adsorption desorption isotherm.

sample	S_{BET} (m^2/g)	V_t (cm^3/g)	V_{meso} (cm^3/g)	V_{mic} (cm^3/g)	V_{mic}/V_t	D_{BJH}(Å)	E_o (kJ/mol)
$\alpha = 0.55$	879	0.554	0.276	0.278	0.50	27	14.4
$\alpha = 0.89$	605	0.523	0.317	0.206	0.39	34	15.4
$\alpha = 1.43$	718	0.622	0.376	0.246	0.40	32	14.3

4.4 Conclusion

In summary, we have developed a template-free synthesis scheme and provided an interfacial reaction mechanism to explain the synthesis of non-spherical colloidal particles in a w/o system. We suggest that for appropriate concentrations of reaction components, anisotropic surface tensions at the w/o interface control the ultimate morphologies of silica particles and promote formation of uniform micro/mesoporous silica ellipsoids.

4.5 References

[1] P.A. Williamson, P.J. Blower, M.A. Green, Chem. Commun. 47 (2011) 1568.

[2] C.T. Kresge, M.E. Leonowicz, W.J. Roth, J.C. Vartuli, J.S. Beck, Nature 359 (1992) 710.

[3] W. Xu, L. Yang, D.L. Akins, J. Phys. Chem. B 106 (2002) 11127.

[4] H.Q. Guo, W. Xu, M.H. Cui, N.L. Yang, D.L. Akins, Chem. Commun. 12 (2003) 1432.

[5] X.M. Zhang, C. Zhang, H.Q. Guo, W.L. Huang, T. Polenova, L.C. Francesconi, D.L. Akins, J. Phys. Chem. B 109 (2005) 19156.

[6] G.M. Andrés, P.J. Jorge, M.L. Luis, Adv. Mater. 22 (2010) 1182.

[7] W. Stöber, A. Fink, E.J. Bohn, J. Colloid Interface Sci. 26 (1968) 62.

[8] M. Grun, I. Lauer, K.K. Unger, Adv. Mater. 9 (1991) 254.

[9] K. Schumacher, P.I. Ravikovitch, A. Du Chesne, A.V. Neimark, K.K. Unger, Langmuir 16 (2000) 4648.

[10] K. Schumacher, M. Grun, K.K. Unger, Microporous Mesoporous Mater. 27 (1999) 201.

[11] Z.G. Teng, Y.D. Han, J. Li, F. Yan, W.S. Yang, Microporous Mesoporous Mater. 127 (2010) 67.

[12] J.C. Zhang, M. Liu, A.F. Zhang, K.F. Lin, C.S. Song, X.W. Guo, J. Solid State Sci. 12 (2010) 267

[13] Y. Yuri, Y. Kasuhisa, Microporous Mesoporous Mater. 93 (2006) 190.

[14] D. Tao, S. Kai, C. Koen, C.H. Tung, Adv.Mater. 21 (2009) 1936.

[15] Y.X. Hu, J.P. Ge, Y.D. Yin, Chem. Commun. 8 (2009) 914.

[16] X.W. Lou, C.L. Yuan, L.A. Archer, Adv. Mater. 19 (2007) 3328.

[17] T.R. Zhang, Q. Zhang, J.P. Ge, G. James, M.W. Sun, Y.S. Yan, Y.S. Liu, C.L. Chang, J.H. Guo, Y.D. Yin, J. Phys. Chem. C 113 (2009) 3168.

[18] J.H. Zhang, H.Y. Liu, Z.L. Wang, N.B. Ming, Chem.-Eur. J. 14 (2008) 4374.

[19] A. Kuijk, A. van Blaaderen, A. Imhof, J. Am. Chem. Soc. 133 (2011) 2346.

[20] H.M. Princen, S.G. Mason, J. Colloid Sci. 20 (1965) 156.

[21] H.M. Princen, S.G. Mason, J. Colloid Sci. 20 (1965) 246.

[22] B.J. Park, E. Furst, Langmuir 26 (2010) 10406.

[23] M. Ryan, J. Fung, D. Kaz, V.N. Manoharan, Materials Today 13 (2010) 34.

[24] B.P. Binks, J.A. Rodrigues, W.J. Frith, Langmuir 23 (2007) 3626.

[25] R. Nagarajan, C.C. Wang, Langmuir 16 (2000) 5242.

4.6 Supplementary information

4.6.1 SEM images

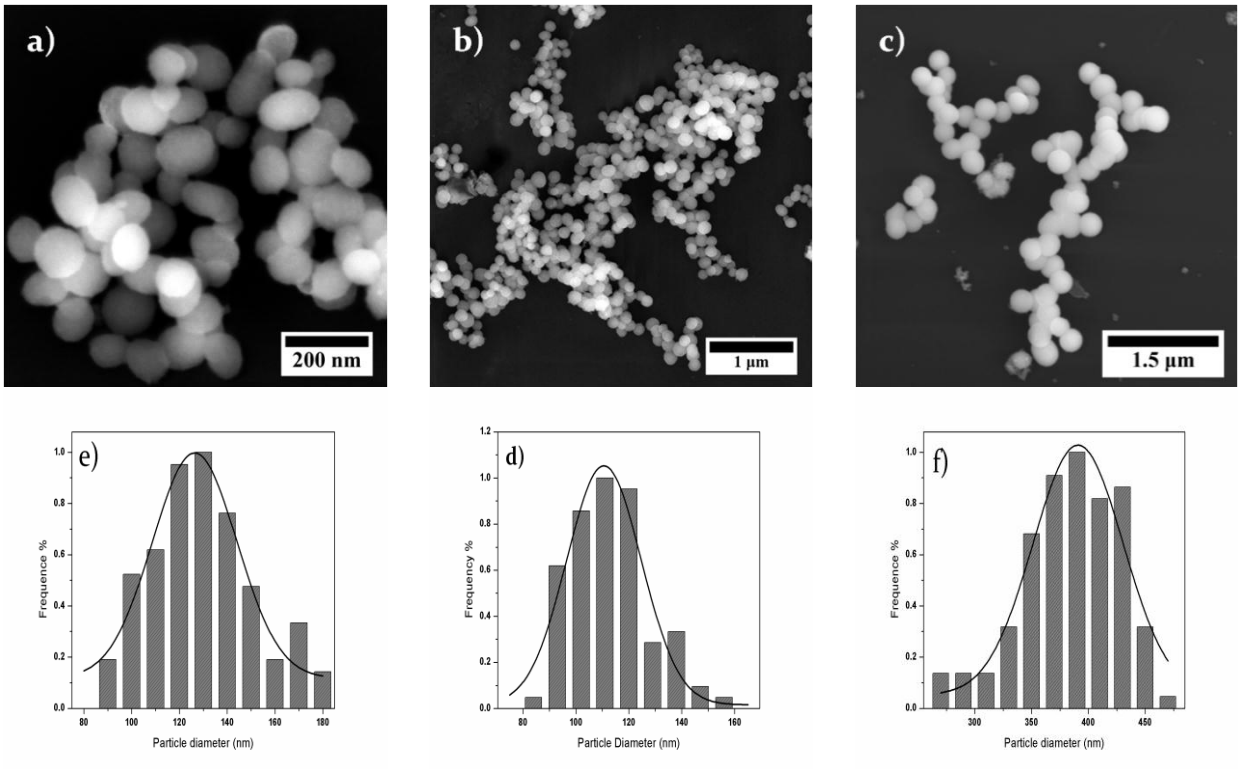

Figure 4-S1. SEM images and particles size analysis of silica nanoparticles synthesized with different volume ratios of water to EG: (a) and (d), α = 1.43; (b) and (e), α = 0.89; (c) and f), α = 0.55.

The shapes of silica particles prepared with different volume ratios of water/ethylene glycol (□ = 1.43, 0.89, and 0.55), as shown in SEM images, are provided in Fig. 4-S1 (a), (b) and (c), respectively. From the SEM images, one can get approximate dimension of the particles: it is found that the mean long axis of silica ellipsoids is approximately 111 nm; and the diameters of the silica spheres are between 124 nm and 375nm. The particle size distribution graphs are given in panels (d), (e) and (f) of Fig. 4-S1.

4.6.2 HR-TEM image

In Fig. 4-S2, an HRTEM image allows determination of the approximate pore size of the porous silica ellipsoids for the sample prepare with $\alpha = 1.43$. As shown in the figure, the diameter of the pore is estimated to be 3.0 nm; which is consistent with the result calculated from the nitrogen desorption/adsorption isotherm using the BJH method (see Fig. 4-S6).

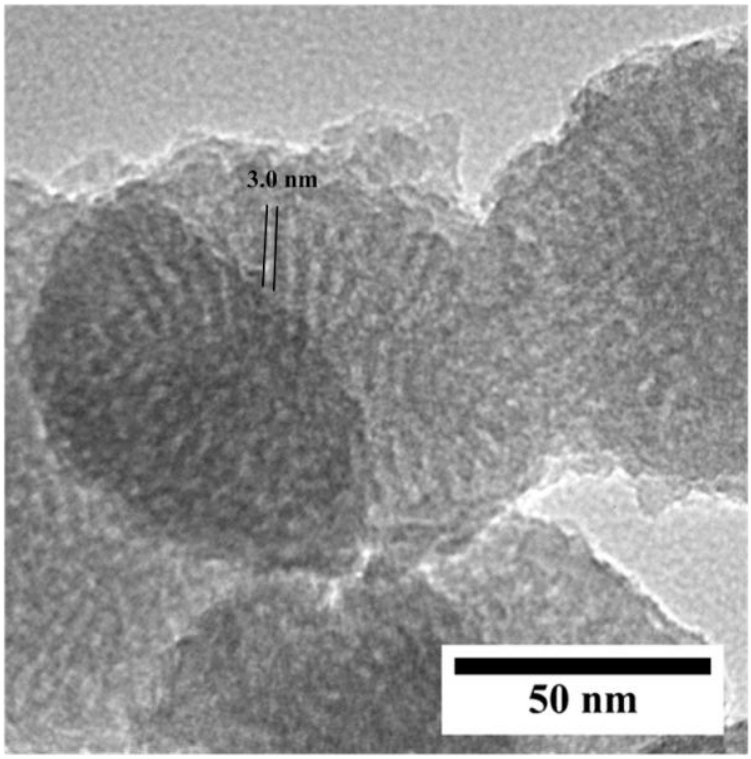

Figure 4-S2. HR-TEM image of mesoporous ellipsoidal silica (volume ratio of water/EG α = 1.43).

4.6.3 FTIR-ATR

Fig. 4-S3 provides the FTIR-ATR spectra for various silica particles prepared under different syntheses. Similar features are found: the intense band at ca. 1100 cm^{-1} is attributed to the transverse-optical mode of the Si-O-Si lattice. Absorption bands associated with the C-H bending vibrations were found between 1350 and 1500 cm^{-1} and between 2850 and 3000 cm^{-1}. It is inferred that, although resultant silica particles have different morphologies, no different chemicals species are formed during reactions.

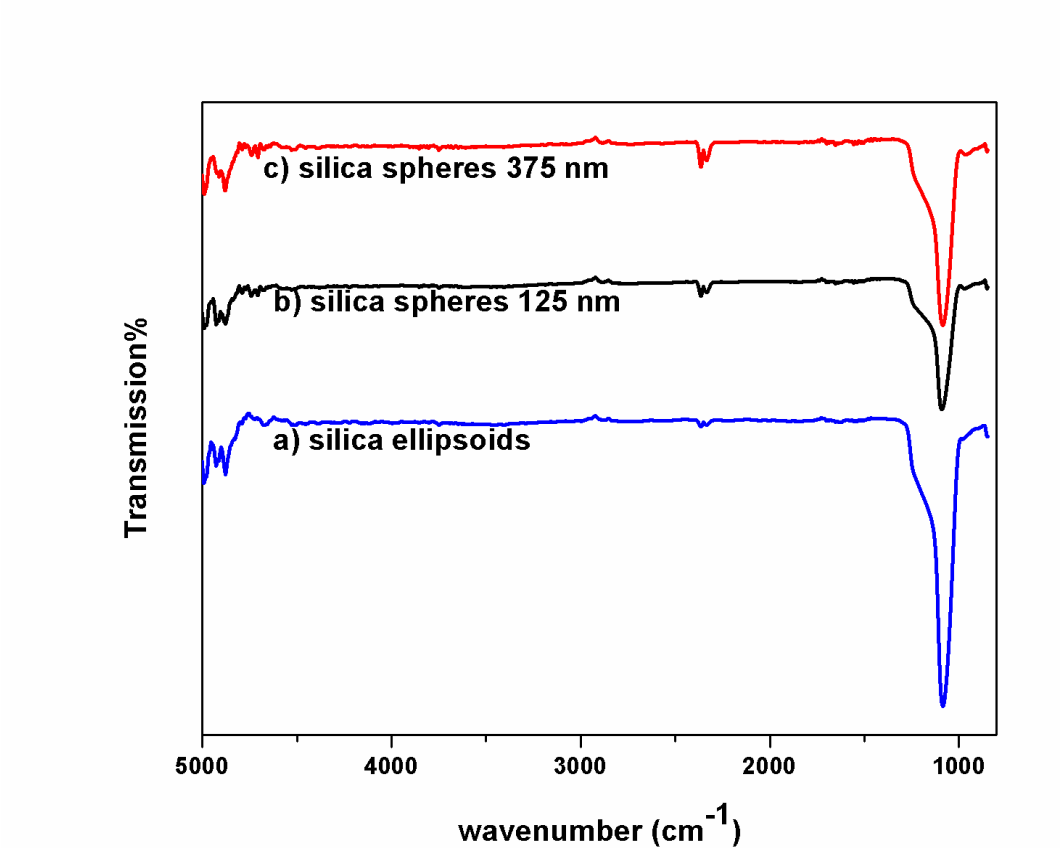

Figure 4-S3. FTIR-ATR spectra of silica particles synthesized with different volume ratios of water to EG: (a) α = 1.43; (b) α = 0.89; and (c) α = 0.55.

4.6.4 XRD

Fig. 4-S4 below shows X-ray diffraction patterns of silica powders prepared using different volume ratios of water and EG. The three samples exhibited a single broad reflection (100), which corresponds to the average pore-pore correlation distance in the small angle region (θ = 1-8). The patterns indicate that the silica products are mesoporous structures. The patterns show that the reflection intensity of spherical silica (curves (a) and (b)) is higher than that of the ellipsoidal silica (curve (c)), also that the reflection intensity increases with gradually decreasing of the volume ratios of water to EG, supporting the view that for the high ratio synthesis (α = 1.43), anisotopic surface tensions are exerted on the nuclei, and the micelles generated by CTAB are altered, with the long range order of mesoporous silica decreased.

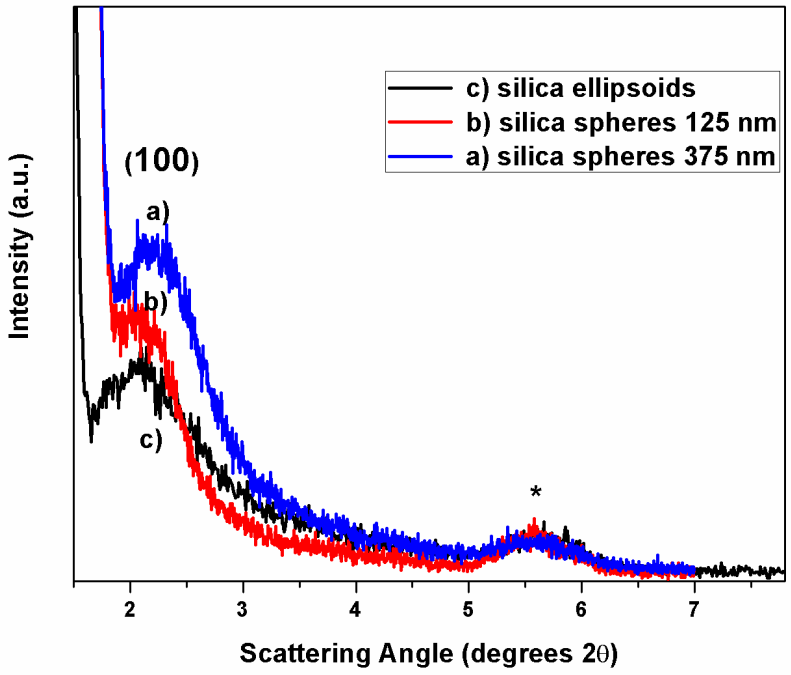

Figure 4-S4. X-ray diffraction patterns of mesoporous silica ellipsoids and silica spheres formed in water-ethylene glycol volume ratios of (a) $\alpha = 0.55$; (b) $\alpha = 0.89$; and (c) $\alpha = 1.43$. (Note: * labels an instrument intrinsic peak that always appears.)

4.6.5 Nitrogen Isotherm and PSDs

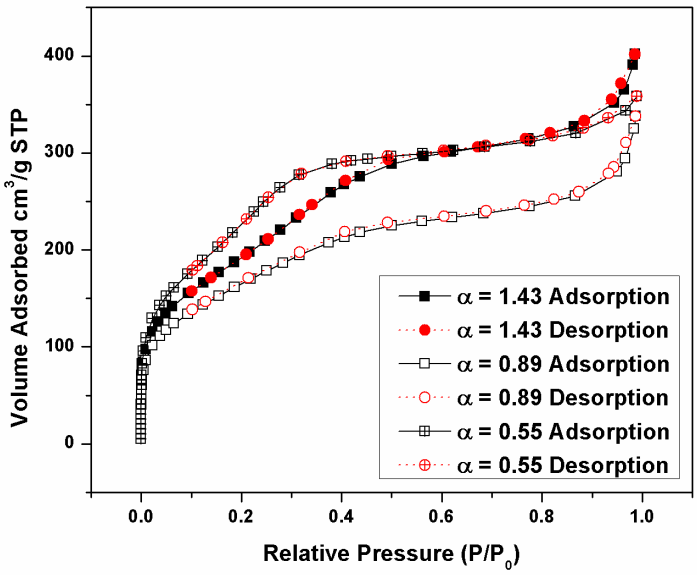

Figure 4-S5. The nitrogen adsorption isotherms of varies morphologies of silica products.

Interestingly, for all three samples, no hysteresis was observed. This suggested that the particles are agglomerated close to one another and the conical wedges between particles can be considered as the most likely predominate shape. The average pore size based on the BJH distribution (see Fig. 4-S6) is shown to be less than 10 % the particle diameter for silica spheres (α = 0.55 and 0.89) and about 30% for the silica ellipsoids (α = 1.43). This difference, once again is linked to the shapes of the particles and their packing/agglomeration in the solids. The pore size of silica ellipsoids is supported by HRTEM measurement (see Fig. 4-S2).

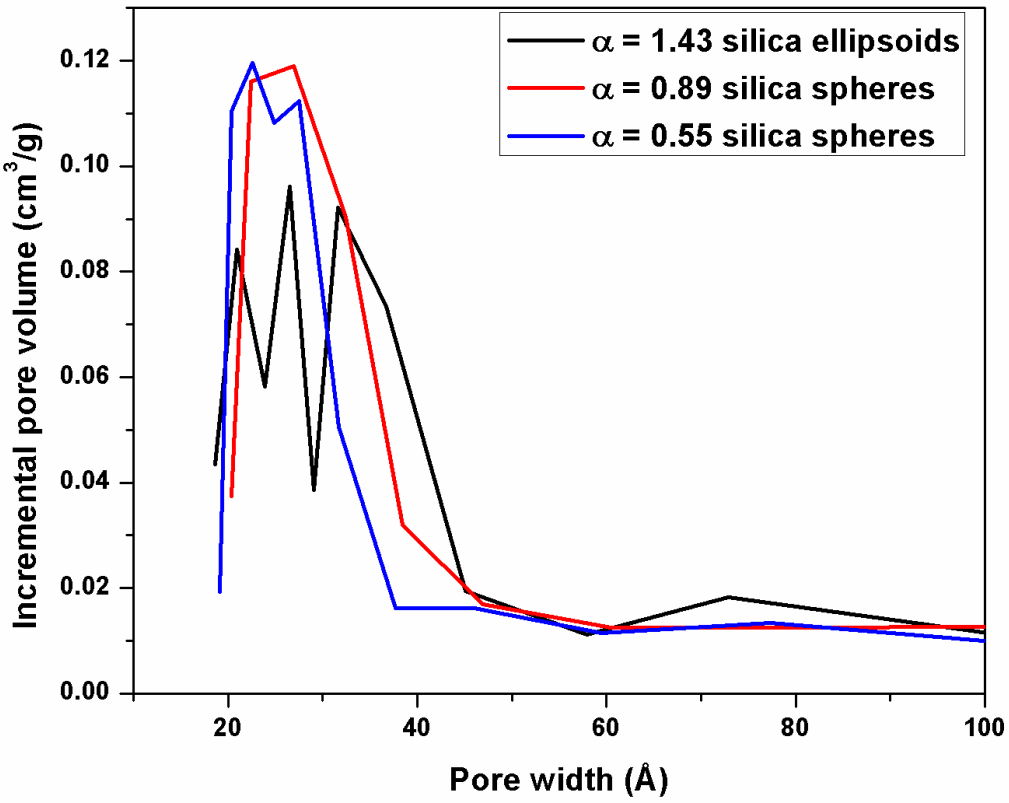

Figure 4-S6. Pore size distribution for silica products.

Chapter 5: Synthesis of hollow ellipsoidal silica nanostructures using a wet-chemical etching approach

5.1. Introduction

A wide range of silica materials have proven interesting from a basic science perspective as well as because of crucial roles such materials play in everyday commercial applications, such as energy storage, chem- and bio-sensors, food processing, drug delivery and catalysis systems [1-6]. In particular, silica colloids (because of the ease of surface functionalization) have proven to be useful absorbent materials in composite structures for enabling controlled porosity, solvent compatibility, and processability [7-9].

Morphologically different silica materials have been created using a broad spectrum of synthesis protocols, including such approaches as soft/hard-templating and the Kirkendall effect [10-15]. The synthesis of spherical silica particles has been the primary focus; the main reason for the present state of affairs is undoubtedly that self-assembled spherical shapes are kinetically favored to occur for most homogeneous synthesis processes. However, unsymmetrical template-assisted approaches may facilitate the formation of uniform, morphologically controllable, non-spherical silica materials [16-18]. It is to be noted that recently, ellipsoidal silica colloidal particles have garnered a great deal of attention because of their use as photonic crystals. In particular, α-Fe_2O_3 spindles have been utilized as templates for fabricating silica ellipsoids, which in turn have been used to form photonic crystals [19]. Also, α-Fe_2O_3/SiO_2 core-shell particles have been converted, through a chemical etching approach, to yolk-shell structures [20,21]. For this latter more complex yolk-shell structure, a shell-by-shell deposition of polycrystalline SnO_2 onto α-

Fe_2O_3/SiO_2 templates has been developed, which resulted in double-walled SnO_2 nano-cocoons [19]. To date, however, although synthesis approaches for formation of unsymmetrical silica particles have been developed, practical applications of such materials are severely limited, largely due to the complexities of preparation processes and the compositional variabilities of the cores.

Another approach to control the morphology of silica particles involves the use of wet-chemical etching. For example, Yin et al. [21] have reported a spontaneous dissolution-regrowth process for fabricating hollow silica spheres. The approach allows the control of surface porosity, as well as minimizes coalescence of nanoparticles, while, because of the porosity, permitting the reactivity of encapsulated catalytic agents to be maintained [21,22]. Shi et al. [23] have used a controllable structural difference-based selective etching strategy to produce nanosized hollow/rattle-type mesoporous silica structures. While He et al. [24] have prepared surface-roughened silica nanoparticles by a self-templating etching route for superhydrophobic coating formation. And, recently, Fang et al. [25] have developed a cationic surface assisted selective etching strategy (CSASE) to produce hollow spherical silica particles with either wormhole-like or oriented mesoporous shells. Generally, in a wet-chemical etching approach, it is found that etching of silica particles leads to the decomposition of the silica and formation of silicate species; the redeposition of silicate at the interior surface of the initial silica particles results in retention of overall shape and, as a result of Ostwald ripening, leads to the formation of hollow silica nanostructures [26].

We utilize a chemical etching approach on prior synthesized ellipsoidal silica nanoparticles (ESNs) [27] in order to fabricate unique ellipsoidal silica shells (ESSs) with dimension less than 100 nm. Compared to prior studies, some of which generated ellipsoidal silica nanoshells using

α-Fe_2O_3 templates, our self-templated, wet-etching approach is an attractive alternate procedure for the following reasons: (i) it is a facile, one-step process that directly produces ellipsoidal silica nanoshells, while overcoming barriers (such as requirement of removing a solid-core template seed) utilized in many reported chemical etching studies; (ii) it results in ellipsoidal silica nanostructures with dimension less than 100 nm; (iii) with an appropriate etchant (e.g., sodium borohydride ($NaBH_4$)), the roughness of the silica shells can be well-controlled, and (iv) results in tunable, uniform size particles with controllable shell thicknesses.

5.2 Materials and Methods

5.2.1 Synthesis of ellipsoidal silica nanoparticles

A typical synthesis process was the following: deionized water and ethylene glycol (Sigma-Aldrich, ReagentPlus® ≥ 99%) solution was prepared; CTAB (Alfa Aesar, 99+ %) was dissolved in the prepared solvent; then 1 M ammonium hydroxide (Pharmco Products, Inc.) was added. After slow addition of TEOS (Acros Organics, 98%), the reaction was held at room temperature with stirring. Following the reaction, the white precipitated was filtered, washed with ethyl alcohol (Decon Labs, Inc., 190 proof), then dried overnight in air at ~60 ºC. The final product was calcination for 8 hrs at ~580 ºC to remove any residual CTAB. The molar ratio of CTAB/NH_4OH/TEOS/ethylene glycol/water was 1:1.2:77.1:381.4:1246.

5.2.2 Synthesis of ellipsoidal silica nanoshells

0.03 g of prior prepared ellipsoidal silica nanoparticles and 0.025 g PVP K29-32 (Acros Organics, M.W. 58,000) were added to a preheated aqueous solvent (50 °C, IKA® ETS-D5) and mixed by mechanical stirring (1,200 rpm) until clear; 0.06 g $NaBH_4$ (Fisher Scientific) was then added to initiate etching, with vigorously stirring for 6 hours. Following the reaction, the silica nanoshells were centrifuged (8,500 rpm) and washed three times with ethyl alcohol. Finally, after drying in air at ~40 ºC overnight, the resultant white powder was collected.

5.2.3 Synthesis of silica-Au nanocomposites

Au nanoparticles were synthesized using the Turkevich method. In a separate reaction, in order to functionalize the silica surface with amino groups, 0.055g of ellipsoidal silica nanoshells (or nanoparticles) were added to a mixture of 15 mL isopropanol (Sigma-Aldrich) and 200 μL of 3-aminopropyltriethoxysilane (APTES) (Acros Organics). The mixture was refluxed at 80 °C for 2 hours with stirring. After cooling to room temperature, the solution was centrifuged (8,500 rpm) and the residue was washed twice with isopropanol then dispersed in water. The citrate stabilized Au nanoparticles were adsorbed onto the amino group functionalized silica colloids by adding the above silica colloids to the Au sols. The solution was sonicated, and then allowed to equilibrate for half-an-hour. The silica-Au nanocomposite was centrifuged and washed with water to remove the unabsorbed Au nanoparticles, and finally dispersed in ethyl alcohol for further characterization.

5.2.4 Characterization

Transmission electron microscopy (TEM, Zeiss EM 902) was performed to observe the sizes and morphologies of silica nanoparticles/nanoshells. To prepare the TEM samples, calcined silica

white powders were dispersed in ethyl alcohol. A 10 µL aliquot of the silica-alcohol solution was dropped onto a carbon-coated copper grid. After evaporation of the alcohol, the sample was characterized by TEM at an acceleration voltage of 80 kV. The same preparation as above was used for scanning electron microscopy (SEM) and energy dispersive X-ray spectrometry (EDS) measurements (using a SEM, Zeiss Supra 55 VP). For the SEM analysis, the voltage was 5 kV and the working distance was between 2 and 5 mm. For the EDS analysis, the voltage was 15 kV and working distance was 8.5 mm.

Fourier-transform infrared (FTIR) spectra were obtained, in the range of 400-5500 cm^{-1}, using a Varian 7000 spectrometer with a resolution of 2 cm^{-1}. A MIRacle single horizontal reflection Attenuated Total Reflectance (ATR) accessory was used in most studies.

Nitrogen adsorption isotherms were measured using an ASAP 2010 analyzer (Micromeritics, Norcross, GA, USA) at -196 °C. Before the experiment, the sample was degassed at 120 °C to a constant pressure of 10^{-4} Torr. The isotherms were used to calculate the specific surface area (S_{BET}), micropore volume (V_{mic}), mesopore volume (V_{mes}), and total pore volume (V_t). Pore size distributions (PSDs) were determined using BJH method.

5.3 Results and discussions

As indicated in the literature, the usual approach for making monodispersed solid and mesoporous silica spheres of tunable sizes involve the Stöber [28] and "modified Stöber" methods [29], respectively. Starting with these basic approaches, and, additionally, by variation of the water/oil (w/o) reaction solution, it has been shown to be possible to vary the shapes of silica particles, and make them spherical, ellipsoidal, rodlike, or cubic; also the size of silica particles have been tuned in the range from nano- to micro-size [18,27].

In this work, meso/microporous silica ellipsoids have been synthesized by controlling the anisotropic surface tension of the reaction solution, and then using chemical etching to morphologically convert nanoparticles to nanoshells. Typical TEM images shows that the resultant silica nanoparticles (see Fig. 5-1a) and silica nanoshells (see Fig. 5-1b) are elliptical in shape. Moreover, the outer dimensions of the nanoshells have been found to be essentially the same as that of their precursor ellipsoidal nanoparticles. Measurements of particles shown in Fig. 5-1a reveal that a typical ellipsoidal silica nanoparticle has a long axis dimension of ~100 nm and an aspect ratio of approximately 4:3. Additionally, we have found that ESSs exhibit a much denser packing than the silica precursors, as indicated by nitrogen adsorption measurements, suggesting the existence of enhanced attractive forces between the nanoshell particles. Specifically, after etching, for the porous structure of the shells, a steep increase in nitrogen adsorption at the relative pressure close to 1 has been observed (as shown in Fig. 5-1c), indicating that nitrogen is prevented from entering the inner-shell surface due to dense packing, which is consistent with the observation of Fig. 5-1b. It is also to be noted that the changes in morphologies of silica particles and shells are indicated by changed porosities (see Table 5-1). Brunauer-Emmett-Teller (BET) measurements of adsorption on our silica samples after etching indicates a decrease of surface area and pore volume, which is due to the removal of silica matrix. Also, the increase of average pore sizes upon conversion of silica particles to shells (~3 nm before etching, ~30 nm after etching), as estimated using the BJH method, demonstrates that the micro-mesoporous structure of the initial silica nanoparticles is changed to shells that contain mesoporous and inter-particular spaces (see Fig. 5-S1).

The molecular structural change of silica ellipsoids before and after chemical etching was also investigated using FTIR-ATR spectroscopy. The intense band at ca. 1086 cm^{-1} (see Fig. 5-1d),

which is attributed to the transverse-optical mode of the Si-O-Si lattice, and the band at ca. 810 cm^{-1}, generally attributed to the Si-O-Si symmetric stretching vibration band, can provide qualitative information on the distance between Si and O atoms [30]. In Fig. 5-1d, FTIR spectra indicate that, the band at 1086 cm^{-1} experiences a red shift of ca. 7 cm^{-1}, from 1086 to 1079 cm^{-1}, while the 801 cm^{-1} band experiences a ca. 10 cm^{-1} red shift, from 811 to 801 cm^{-1}, suggesting that upon formation of silica nanoshells a more open network (Si-O-Si bond) results [31].

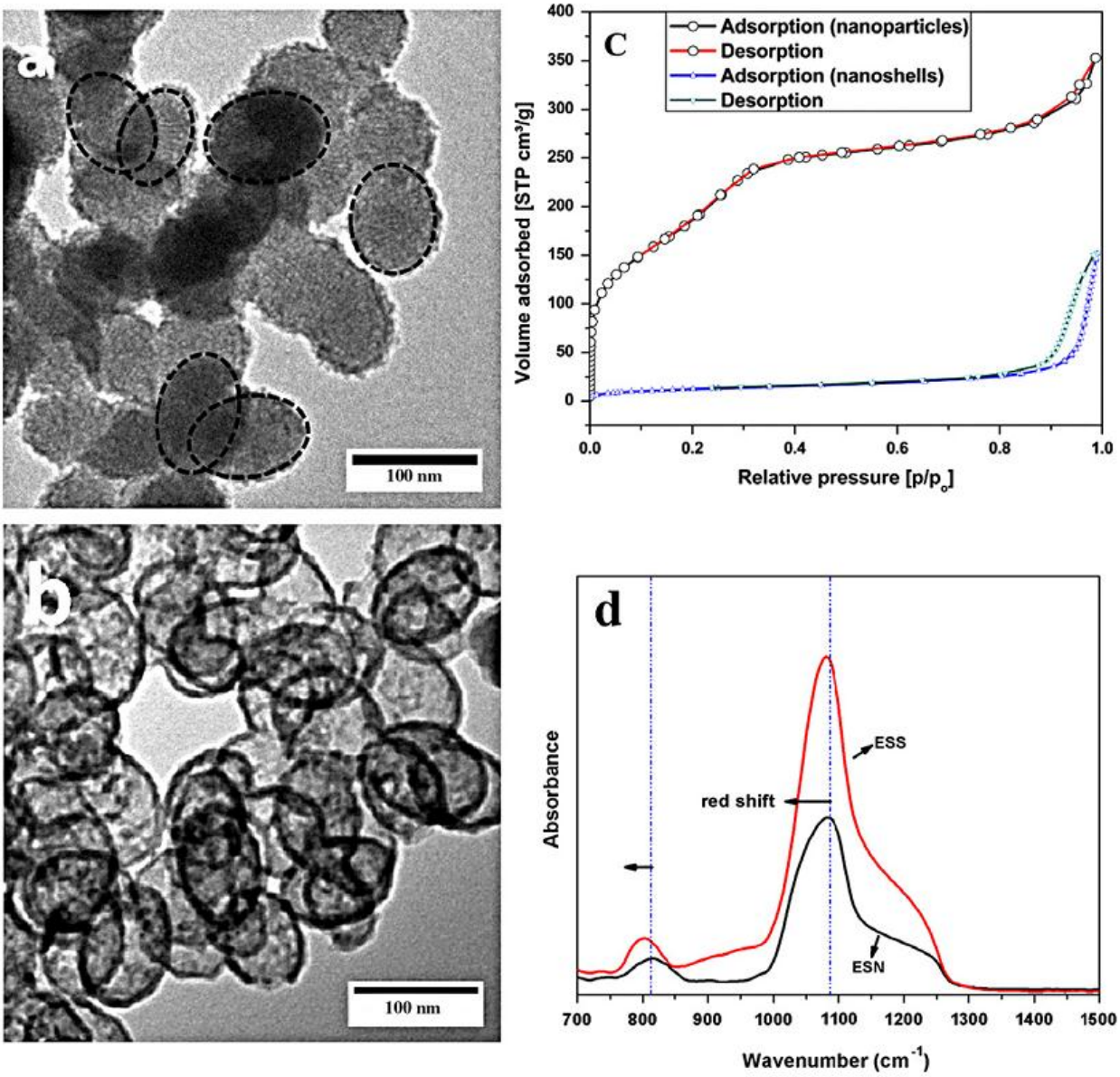

Figure 5-1. TEM images of (a) ellipsoidal silica nanoparticles (ESNs); (b) ellipsoidal silica nanoshells (ESSs); (c) Nitrogen adsorption isotherms of ellipsoidal silica nanoparticles (ESNs) and ellipsoidal silica nanoshells (ESSs); and (d) FTIR-ATR spectra of ESNs and ESSs.

Table 5-1. Parameters of the pore structure calculated from nitrogen adsorption isotherms.

Sample	S_{BET} (m^2/g)	V_t (cm^3/g)	V_{meso} (cm^3/g)	V_{mic} (cm^3/g)	D_{BJH}	V_{mic}/V_t
ESSs	43	0.239	0.223	0.016	253	0.07
ESNs	718	0.622	0.376	0.246	32	0.40

In order to further demonstrate control of the morphologies of the silica particles, a range of initial experimental conditions were utilized. As shown in Fig. 5-2a and 5-2c, ESSs are obtained upon synthesis at a temperature of ~50 °C, while Fig. 5-2b and 5-2d shows that for the same amounts of initial reagents, but at a higher temperature of about ~80 °C, silica shells of about twice the thickness are obtained. More detailed study shows that upon adjusting the temperature from 50 °C (see Fig. 5-2a) to 60 °C (see Fig. 5-1b), and subsequently to 80 °C (see Fig. 5-2c), the thicknesses of the silica nanoshells have the values ~4, 6 and 8 nm, respectively, as calculated from TEM images. A plausible interpretation of the factors responsible for the observed thicknesses is that both the decomposition and condensation rates should increase at higher temperature, with condensation occurring at a faster rate, leading to the formation (for appropriate concentrations) of a silica shell. This latter eventuality is supported by SEM measurements, where the orifices in the shell in the high temperature regime can be clearly observed (see Fig. 5-S2).

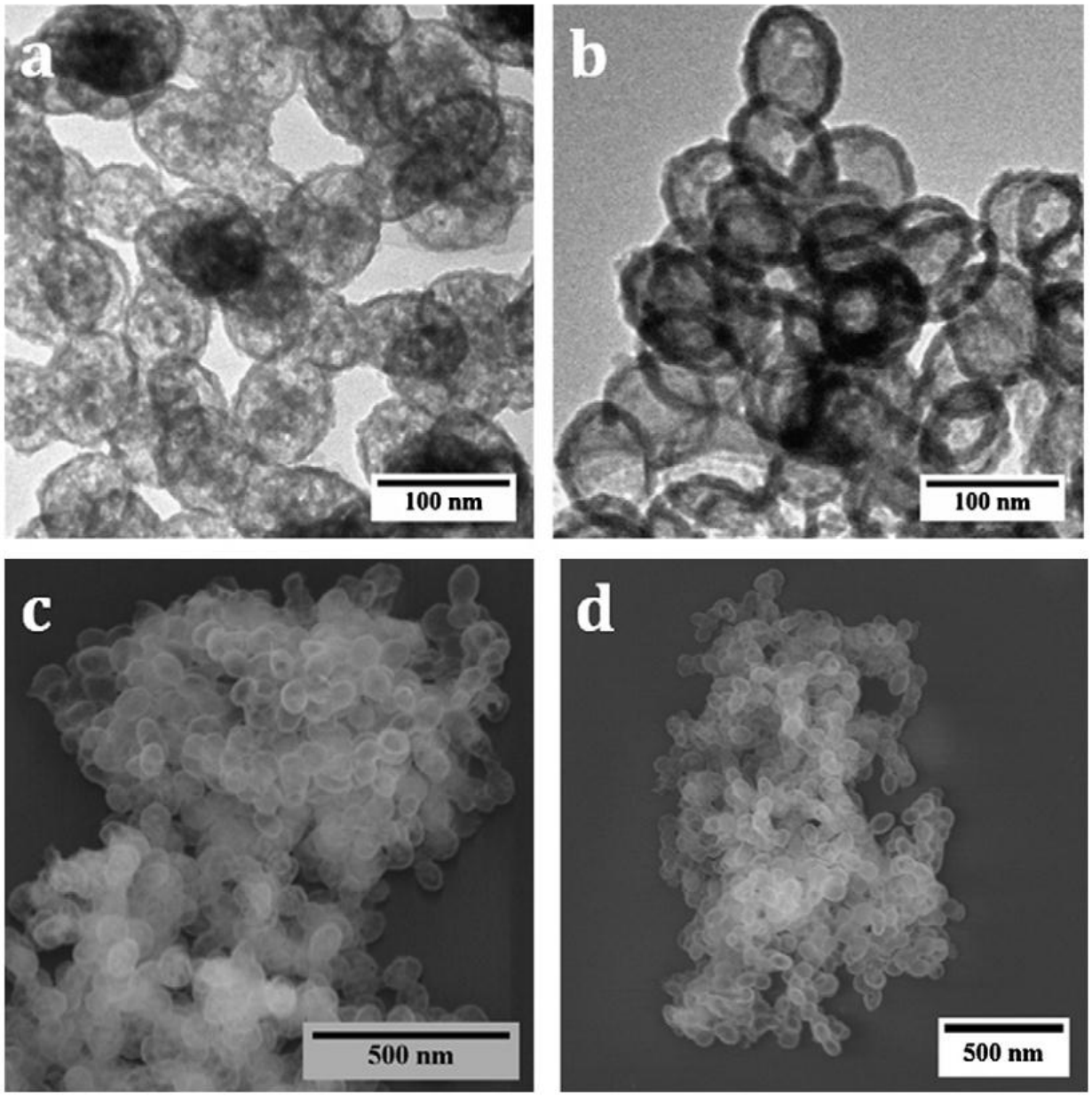

Figure 5-2. TEM and SEM images for different syntheses conditions: (a) and (c) mass ratio of silica particles/PVP/$NaBH_4$ is 1.2:1: 2.4, reaction temperature ~50 °C; (b) and (d) mass ratio of silica particles/PVP/$NaBH_4$ is 1.2:1:2.4, reaction temperature ~80 °C.

It is known that wet-chemical etching of silica materials occurs for both acidic and basic etchants [22,32]. And, as is to be expected, some etchants are not appropriate for various reasons; as an example, although potassium cyanide (KCN) can be used to thin silica shells, its high toxicity limits its use [32]. Beyond just using a simple etchant, the strategy is to use it in combination with a protective coating of the surface (i.e., "surface protected etching"; using PVP, for example) to maintain particle integrity [20,22]. In our etching process, we have used $NaBH_4$ as the etchant and PVP as the protecting agent. We have ascertained that besides the aforementioned temperature effects on the resultant morphologies, variation of the other synthesis conditions can control the ultimate morphologies of silica nanostructures. For example, when small amounts of silica ellipsoidal particles were introduced, the silicate species does not reach the supersaturation level, leading to amorphous silica being obtained. And upon increasing the silica particle concentration above a certain level (amount ESNs ~0.03g), ellipsoidal silica nanoshells are formed as shown in Fig. 5-3b. Also, upon increasing the amount of participant silica ellipsoids, everything else held constant, only partially etched silica particles are formed, as shown in Fig. 5-3c.

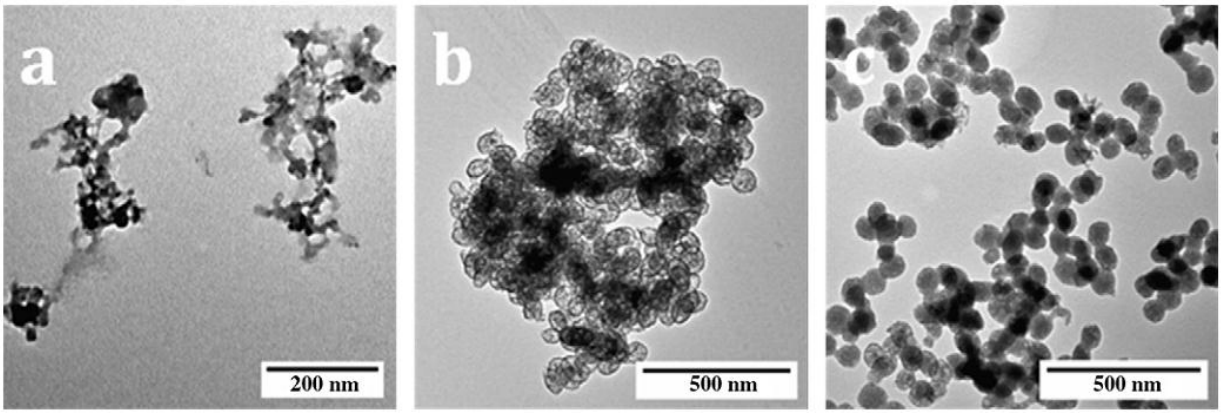

Figure 5-3. TEM images of different synthesis reaction samples. (a) Mass ratio of silica particles/PVP/$NaBH_4$ of 0.4:1: 2.4, reaction temperature of ~50 °C; (b) mass ratio of silica particles/PVP/$NaBH_4$ is 1.2:1:2.4, reaction temperature of ~50 °C; (c) mass ratio of silica particles/PVP/$NaBH_4$ is 4.0:1: 2.4, reaction temperature of ~50 °C.

In order to further investigate the morphological effect of the etchant and PVP, as a reference, ellipsoidal nanoshells were generated using $NaBH_4$ at a concentration of ~0.06 g and PVP at ~0.025 g (see Fig 5-2a). We observed that when an appropriate amount PVP was used, e.g., ~0.01 g, silica ellipsoidal nanoshells of very thin shell thickness were obtained, as shown in Fig. 5-4a. And upon adding ~0.025 g of PVP, everything else being the same, only ellipsoidal shells were formed. Moreover, on increasing the amount of PVP even further, to ~0.1 g, etching is blocked, as shown in Fig. 5-4b, likely due to the decrease in the quantity of OH^- ions that penetrate the highly protected silica surface. Also, we have found that upon increasing the amount of $NaBH_4$, for example to ~0.1 g as shown in Fig. 5-4c, very thin, partial ellipsoidal nanoshells were formed. We explain this observation as the result of increased OH^- concentration when more $NaBH_4$ is added. The increased amount of OH^- is theorized to promote the decomposition of the condensed silica, resulting in silica particles of less uniform structures. And, indeed, increase of the amount of $NaBH_4$ even further (as shown in Fig. 5-4d) would be expected to lead to the absence of hollow particles altogether.

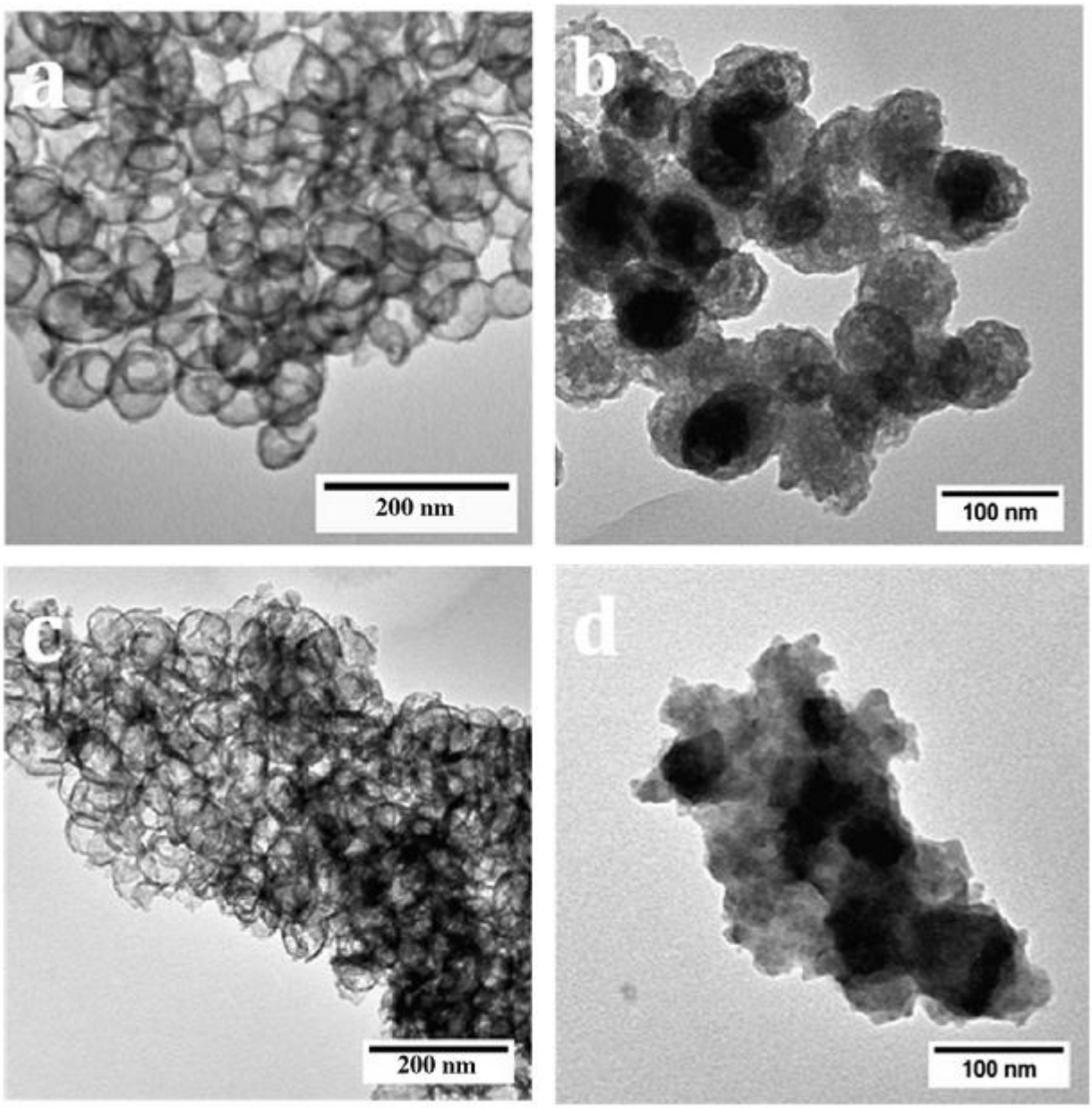

Figure 5-4. TEM images of different synthetic conditions samples. (a) mass ratio of silica particles/PVP/$NaBH_4$ is 1.2:0.4:2.4, reaction temperature ~50 °C; (b) mass ratio of silica particles/PVP/$NaBH_4$ is 1.2: 4:2.4, reaction temperature ~50 °C; (c) mass ratio of silica particles/PVP/$NaBH_4$ is 1.2:1:4, reaction temperature ~50 °C; (d) mass ratio of silica particles/PVP/$NaBH_4$ is 1.2:1:8, reaction temperature ~50 °C.

Even though the mechanism for conversion of solid spherical silica to spherical shells has been dealt with in the literature [20,21,23], it is still a challenge to fabricate silica nanoparticles with dimension less than 100 nm, largely due to the difficulties of controlling the basic etching additives. A schematic mechanism describing how ellipsoidal nanoshells may be formed is provided in Fig. 5-5. In our mechanism, the porous structure on the surface of the ESNs provides a pathway for the etchant (OH^-) to penetrate into the core of the silica material, thus facilitating even more etching. And when silicates reach the supersaturation level at the interface, condensation is expected to occur, leading to the expansion of the inner shell while maintaining the overall ellipsoidal shape. In our mechanism, the porous texture of silica particles is essential for formation of nanoscaled shells resulting from the acceleration associated with the penetration of etchants. As a test of the proposed mechanism in which the porosity leads to inner surface silicate formation with retention of overall shape of the initial silica nanoparticles, we used the wet chemical etching approach to synthesize nanoshells starting with solid spherical silica particles. Upon applying the same synthesis conditions, the resultant silica particles show only a roughened surface, with no formation of hollow shells (as shown in Fig. 5-S3).

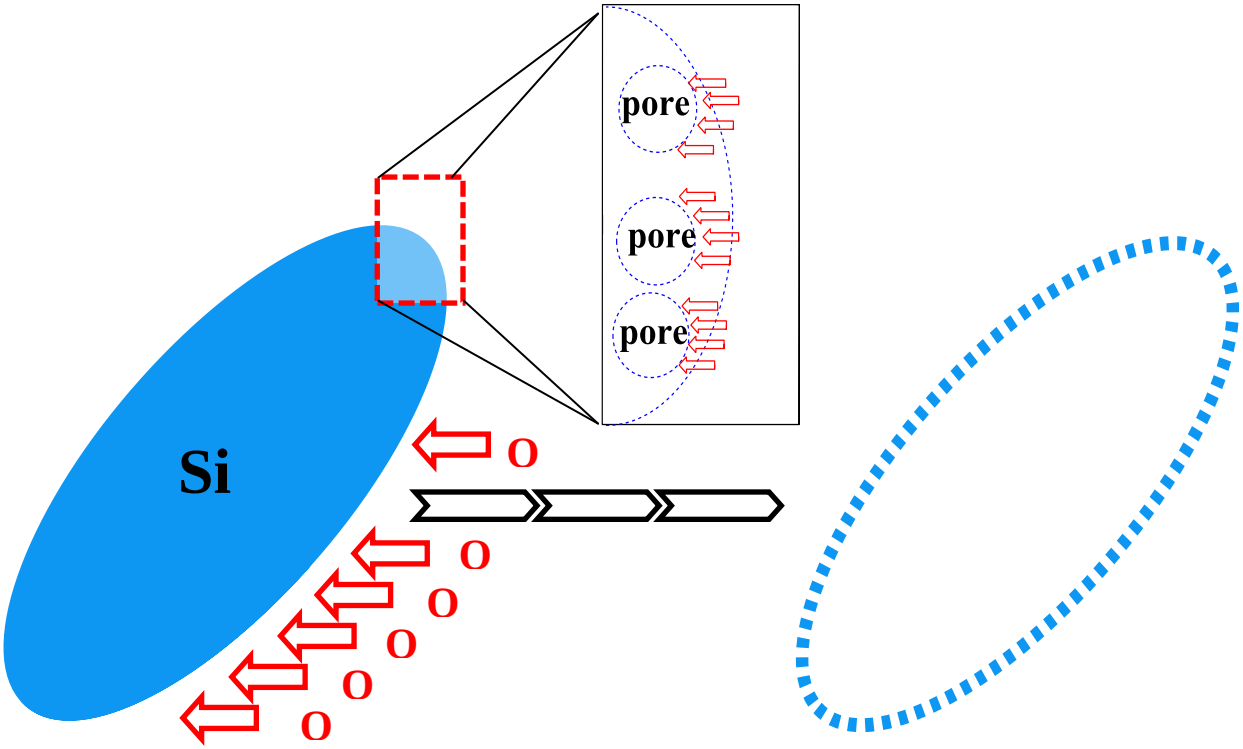

Figure 5-5. Schematic mechanism for formation of ESSs (figure represents 2-dimensional slice through the 3-dimensional structure).

In this work we present a facile approach for generating mesoporous as well as nanoshell ellipsoidal silica nanostructures that have enormous potential for use in important application areas dealing with catalysis, hydrogen storage and sensor. Moreover, in pursuing our experimental ends we have dealt with the synthesis of spherical silica-metal nanocomposites of various sizes, shapes and compositions, and briefly present our preliminary results here. Specifically, Au nanoparticles (NPs) of ~7 nm diameter have been attached onto ellipsoidal silica nanoparticles and ellipsoidal silica nanoshells. For our nanocomposite system, surface functionalization using a silanization agent (APTES) was use to allow a substantial mass percentage of Au NPs to be incorporated. As shown in panels 6a and 6b of Fig. 5-6, Au NPs are attached onto the surface of ellipsoidal silica nanoparticles, with the highest mass ratio attained being 14.5%. We also have, as shown in panels 6c and 6d, attached the Au NPs onto the surface of nanoshell ellipsoidal silica nanostructures. It is to be noted that surface stabilization, as described herein, as opposed to within the channels of mesoporous materials, avoids Au NPs growth within channels, which would somewhat limit chemical reactivity.

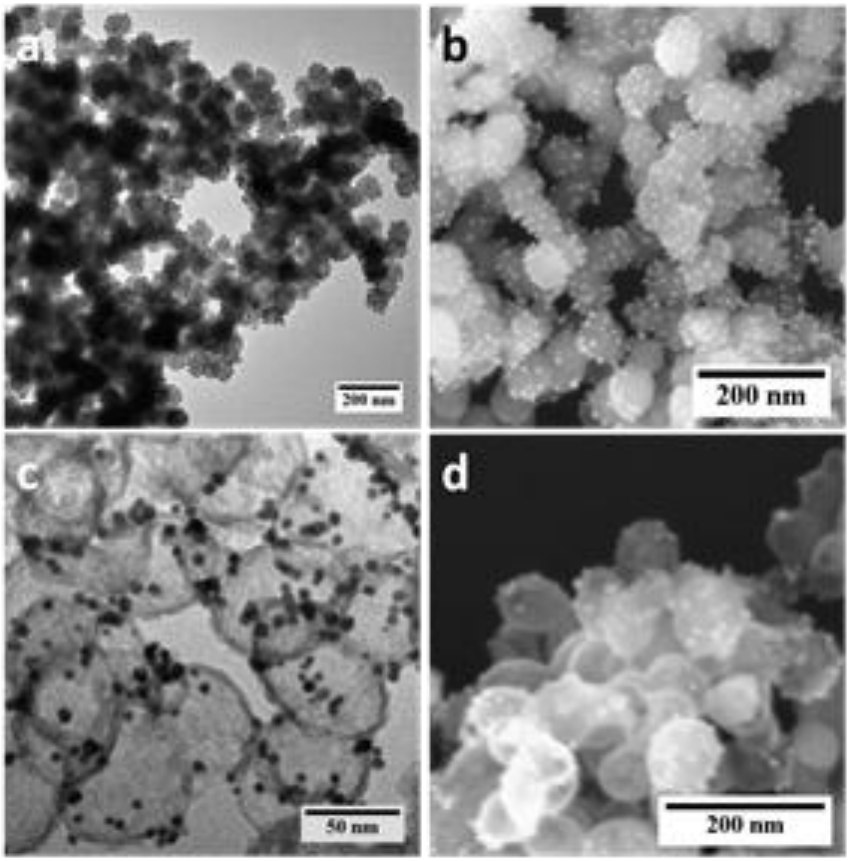

Figure 5-6. (a) and (b), respectively, TEM and SEM images of ellipsoidal silica nanoparticles-Au nanocomposite; (c) and (d), respectively, TEM and SEM images of ellipsoidal silica nanoshells-Au nanocomposite.

5.4 Conclusion

In summary, we have developed a chemical etching approach for syntheses of ellipsoidal silica nanoshells of controllable shell thicknesses. The hollow nanostructures were derived from precursor porous ellipsoidal silica nanoparticles by carefully regulating the synthesis conditions. It is hypothesized that the small pores of silica ellipsoids provide pathways for the etchant to penetrate, which facilitates internal etching, leading to form silica shells.

5.5 References

[1] Q.J. He, J.L. Shi, J. Mater. Chem. 21 (2011) 5845.

[2] S. Bonacchi, D. Genovese, R. Juris, M. Montalti, L. Prodi, E. Rampazzo, N. Zaccheroni, Angew. Chem. Int. Ed. 50 (2011) 4056.

[3] G.M. Andrés, P.J. Jorge, M.L. Luis, Adv. Mater. 22 (2010) 1182.

[4] H.Q. Guo, W. Xu, M.H. Cui, N.L. Yang, D.L. Akins, Chem. Commun. 12 (2003) 1432.

[5] X.M. Zhang, C. Zhang, H.Q. Guo, W.L. Huang, T. Polenova, L.C. Francesconi, D.L. Akins, J. Phys. Chem. B 109 (2005) 19156.

[6] M. Roca, A.J. Haes, J. Am. Chem. Soc. 130 (2008) 14273.

[7] Y. Yamada, M. Mizutani, T. Nakamura, K. Yano, Chem. Mater. 22 (2010) 1695.

[8] R.A. Caruso, M. Antonietti, Chem. Mater. 13 (2001) 3272.

[9] L.M. Liz-Marzan, P. Mulvaney, in Surfactant Science Series, ed. U. Zoller, Taylor & Francis, London. 2006.

[10] F. Caruso, R.A. Caruso, H. MÖhwald, Science 282 (1998) 1111.

[11] Y.D. Yin, R.M. Rioux, C.K. Erdonmez, S. Hughes, G.A. Somorjai, A.P. Alivisatos, Science 304 (2004) 711.

[12] Y.G. Sun, Y.N. Xia, J. Am. Chem. Soc. 126 (2004) 3892.

[13] M.H. Yu, H.N. Wang, X.F. Zhou, P. Yuan, C.Z. Yu, J. Am. Chem. Soc. 129 (2007) 14576.

[14] J.G. Wang, F. Li, H.J. Zhou, P.C. Sun, D.T. Ding, T.H. Chen, Chem. Mater. 21 (2009) 612.

[15] J. Liu, S.B. Hartono, Y.G. Jin, Z. Li, G.Q. Lu, S.Z. Qiao, J. Mater. Chem. 20 (2010) 4595.

[16] D. Tao, S. Kai, C. Koen, C.H. Tung, Adv.Mater. 21 (2009) 1936.

[17] Y.X. Hu, J.P. Ge, Y.D. Yin, Chem. Commun. 8 (2009) 914.

[18] A. Kuijk, A. van Blaaderen, A. Imhof, J. Am. Chem. Soc. 133 (2011) 2346.

[19] X.W. Lou, C.L. Yuan, L.A. Archer, Adv. Mater. 19 (2007) 3328.

[20] T.R. Zhang, Q. Zhang, J.P. Ge, G. James, M.W. Sun, Y.S. Yan, Y.S. Liu, C.L. Chang, J.H. Guo, Y.D. Yin, J. Phys. Chem. C 113 (2009) 3168.

[21] T.R. Zhang, J.P. Ge, Y.X. Hu, Q. Zhang, Y.D. Yin, Angew. Chem. Int. Ed. 47 (2008) 5806.

[22] Q. Zhang, T.R. Zhang, J.P. Ge, Y.D. Yin, Nano Lett. 8 (2008) 2867.

[23] Y. Chen, H.G. Chen, L.M. Guo, Q.J. He, F. Chen, J. Zhou, J.W. Feng, J.L. Shi, ACS Nano 4 (2010) 529.

[24] X. Du, J.H. He, ACS Appl. Mater. Interfaces 3 (2011) 1269.

[25] X.L. Fang, C. Chen, Z.H. Liu, P.X. Liu, N.F. Zheng, Nanoscale 3 (2011) 1632.

[26] B. Liu, H.C. Zeng, Small, 5 (2005) 566.

[27] H.N. Zhang, T.J. Bandosz, D.L. Akins, Chem. Commun. 47 (2011) 7791.

[28] W. Stober, A. Fink, E.J. Bohn, J. Colloid Interface Sci. 26 (1968) 62.

[29] M. Grun, I. Lauer, K.K. Unger, Adv. Mater. 9 (1991) 254.

[30] S. Bruynooghe, F. Bertin, A. Chabli, J.C. Gay, B. Blanchard, M. Couchaud, Thin Solid Films 313 (1998) 722.

[31] H. Zhu, Y.G. Ma, Y.G. Fan, J.C. Shen, Thin Solid Films 397 (2001) 95.

[32] Y.L. Shi, T. Asefa, Langmuir 23 (2007) 9455.

5.6 Supplementary information

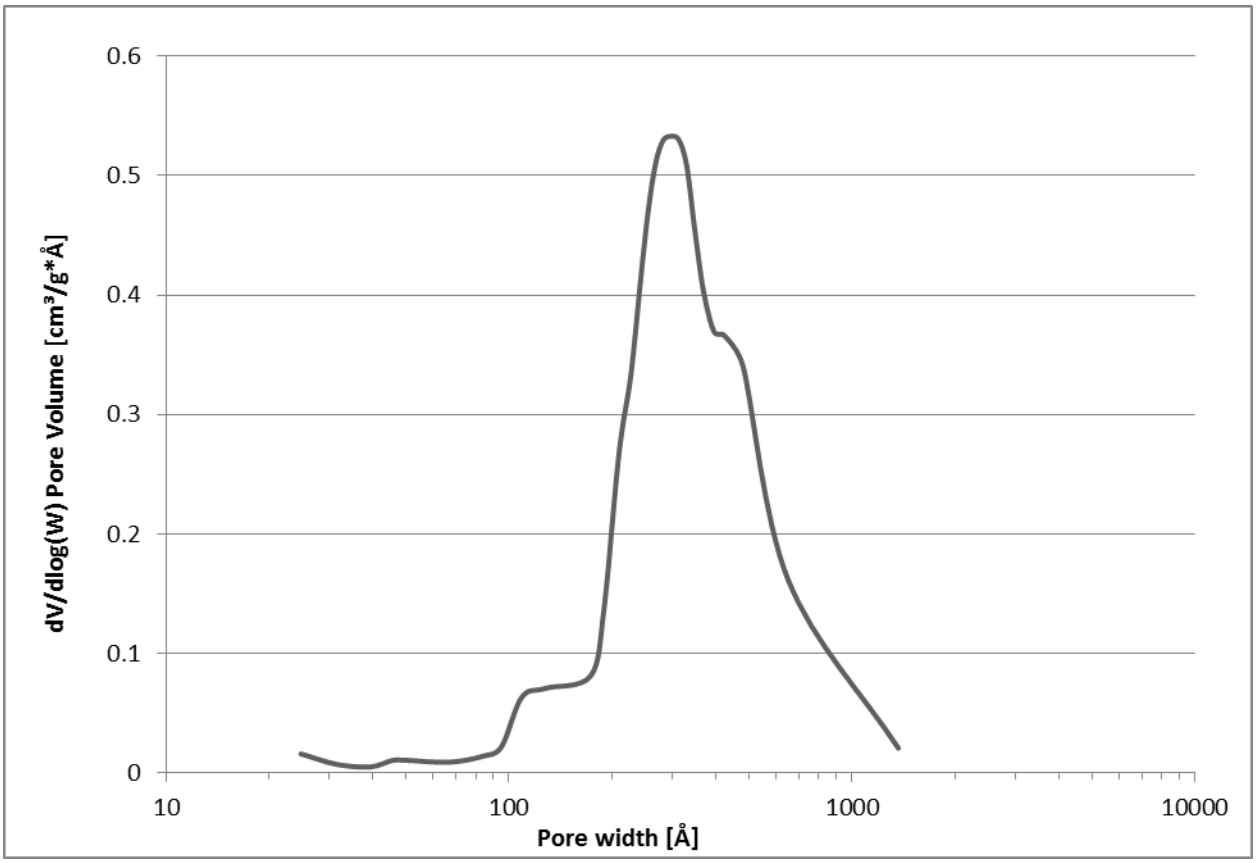

Figure 5-S1. Pore size distributions (PSDs) of ellipsoidal silica nanoshells calculated by BJH method.

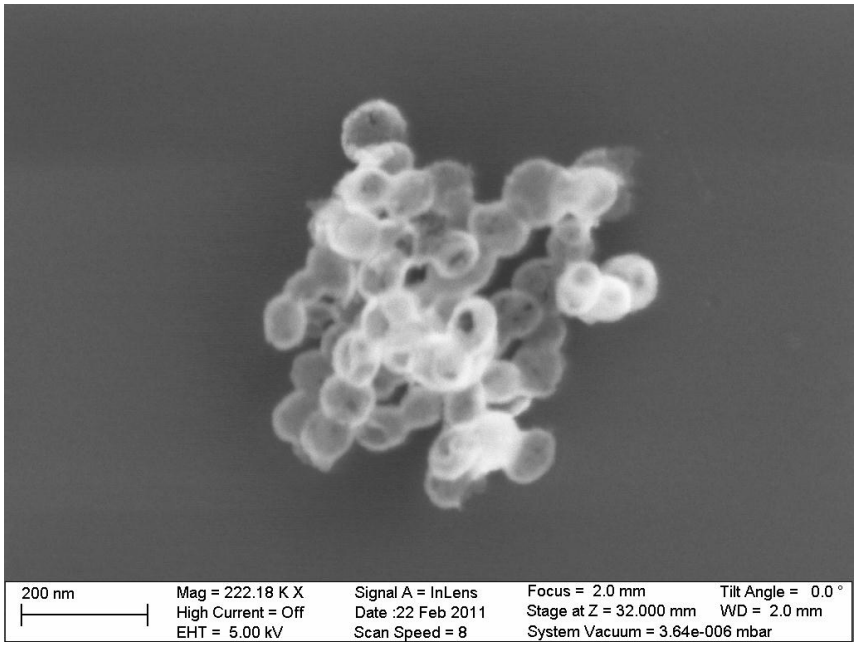

Figure 5-S2. SEM image showing defects (holes) in ellipsoidal silica nanoshells that were synthesized at reaction temperature ~80 °C and mass ratio of silica particles/PVP/$NaBH_4$ of 1.2:1:2.

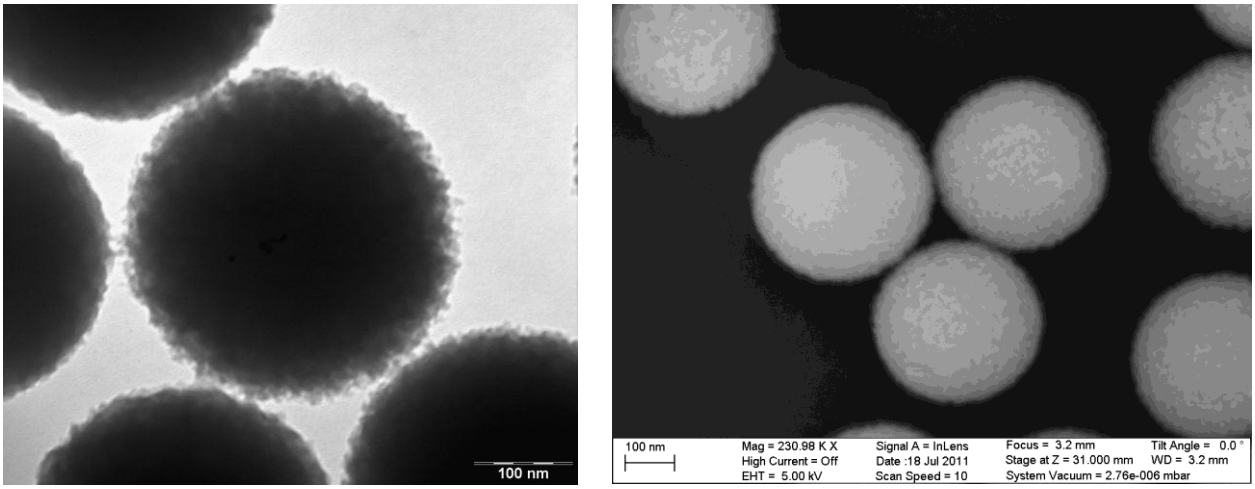

Figure 5-S3. TEM and SEM images show the resultant morphologies of solid spherical silica particles that were synthesized using the wet-chemical etching approach that we have developed.

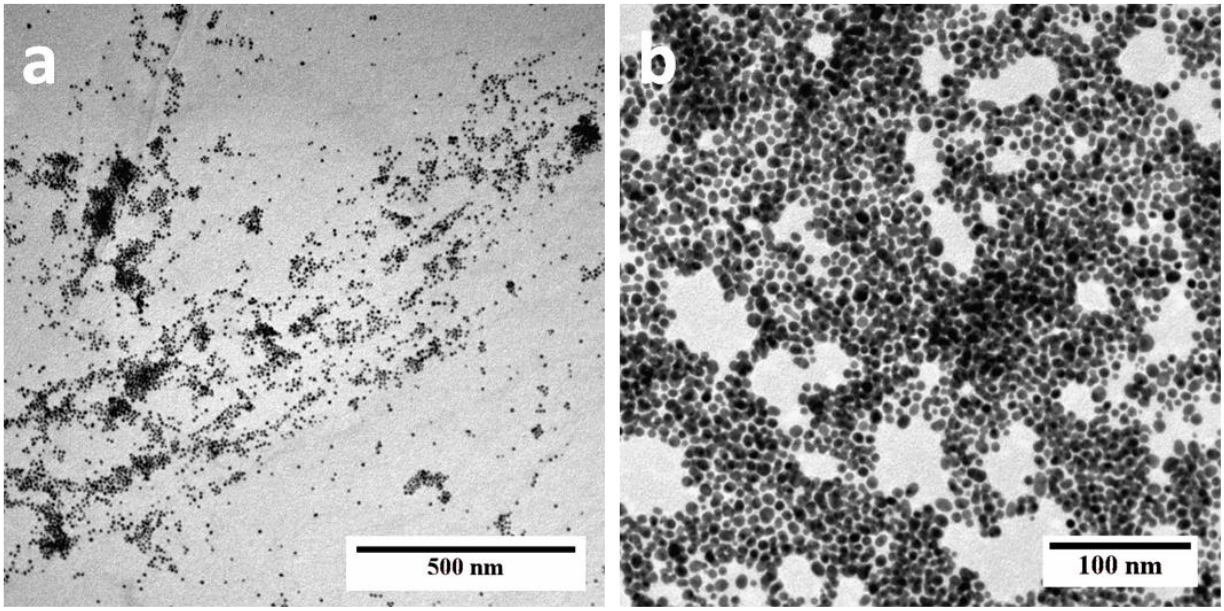

Figure 5-S4. TEM images of Au nanoparticles at different magnifications.

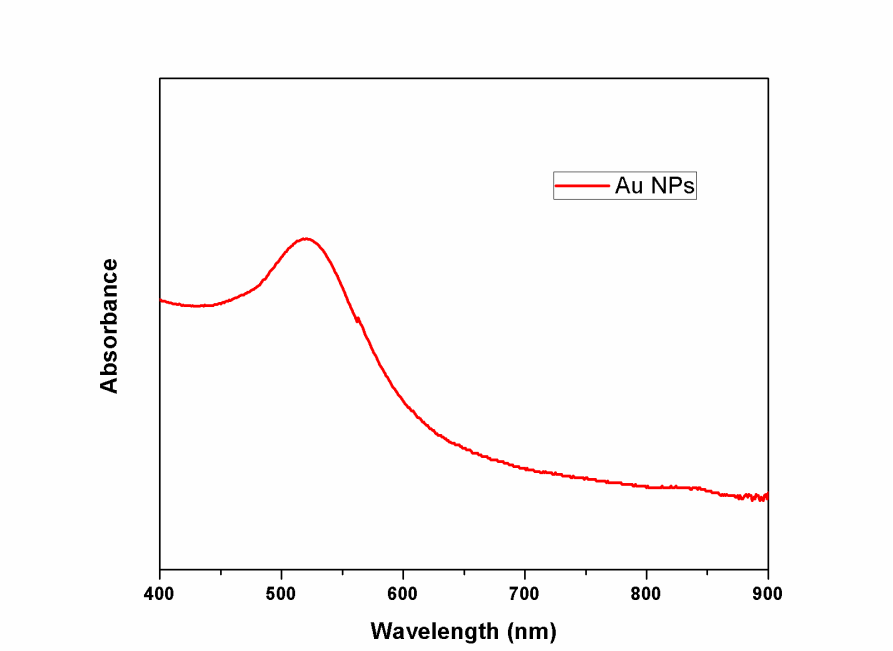

Figure 5-S5. UV-Vis spectrum of Au nanoparticles.

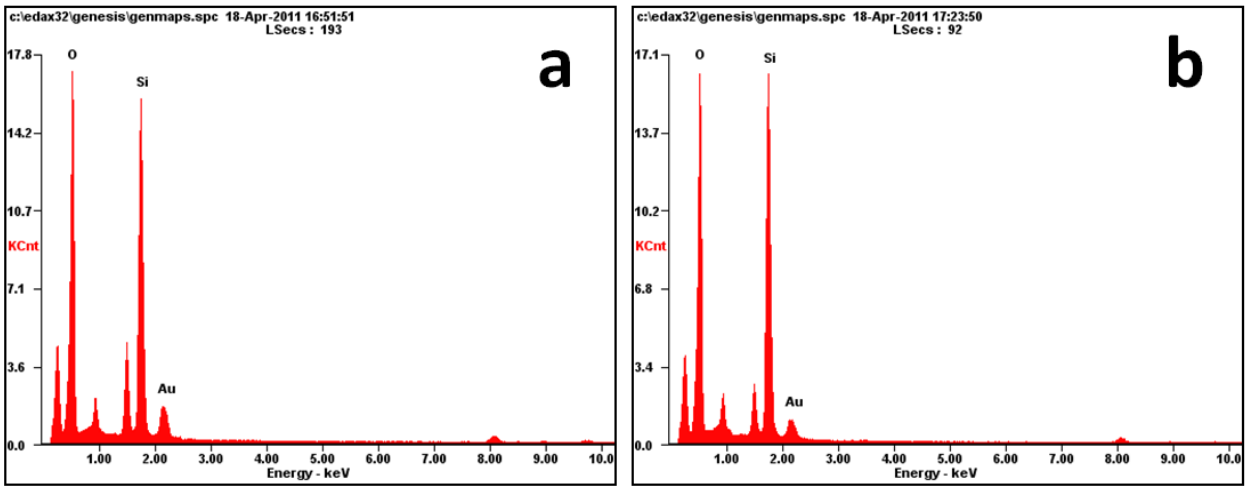

Figure 5-S6. EDX reveals the elemental content of (a) ellipsoidal silica nanoparticles, and (b) nanoshells composites. (a) The Au element mass content is 14.46%; (b) the Au element mass content is 8.78%.

Bibliography

Chapter 1

[1] Q.J. He, J.L. Shi, J. Mater. Chem. 21 (2011) 5845.

[2] S. Bonacchi, D. Genovese, R. Juris, M. Montalti, L. Prodi, E. Rampazzo, N. Zaccheroni, Angew. Chem. Int. Ed. 50 (2011) 4056.

[3] G.M. Andrés, P.J. Jorge, M.L. Luis, Adv. Mater. 22 (2010) 1182.

[4] M. Roca, A.J. Haes, J. Am. Chem. Soc. 130 (2008) 14273.

[5] Y. Yamada, M. Mizutani, T. Nakamura, K. Yano, Chem. Mater. 22 (2010) 1695.

[6] R.A. Caruso, M. Antonietti, Chem. Mater. 13 (2001) 3272.

[7] F. Caruso, R.A. Caruso, H. MÖhwald, Science 282 (1998) 1111.

[8] Y.D. Yin, R.M. Rioux, C.K. Erdonmez, S. Hughes, G.A. Somorjai, A.P. Alivisatos, Science 304 (2004) 711.

[9] Y.G. Sun, Y.N. Xia, J. Am. Chem. Soc. 126 (2004) 3892.

[10] H.N. Zhang, T.J. Bandosz, D.L. Akins, Chem. Commun. 47 (2011) 7791.

[11] L.L. Hench, J.K. West, Chemical Reviews 90 (1990) 33.

[12] J.M. Seddon, R.H. Templer. Handbook of Biological Physics, Vol. 1, ed. R. Lipowsky, E. Sackmann. (c) 1995, Elsevier Science B.V.

[13] M. Volpert, European Synchrotron Radiation Facility (ESRF), <http://scitech.web.cern.ch/scitech/deeperdown/surfactant.html > (visited 18 September, 2012).

[14] C.T. Kresge, M.E Leonowicz, W.J. Roth, J.C. Vartuli, J.S. Beck, Nature 359 (1992) 710.

[15] V. Alfredsson, M.W. Anderson, Chem. Mater. 8 (1996) 1141.

[16] D. Zhao, J. Feng, Q. Huo, N. Melosh, G.H. Fredrickson, B.F. Chmelka, G.D. Stucky, Science 279 (1998) 548.

[17] N.K. Raman, M.T. Anderson, C.J. Brinker, J. Chem. Mater. 8 (1996) 1682.

[18] A. Sayari, P. Liu, Microporous Mater. 12 (1997) 149.

[19] J.S. Beck , J.C. Vartuli , W.J. Roth , M.E. Leonowicz , C.T. Kresge , K.D. Schmitt , C.T. W. Chu , D.H. Olson , E.W. Sheppard, J. Am. Chem. Soc. 114 (1992) 10834.

[20] W. Ostwald, Lehrbuch der Allgemeiene Chemie, V.1 P. 1 (1896) Leipzig, Germany.

[21] N. Miyata, H. Watanabe, M. Ichikawa, Appl. Phys. Lett. 73 (1998) 3923.

[22] T. Zhang, J. Ge, Y. Hu, Q. Zhang, S. Aloni, Y. Yin, Angew. Chem. Int. Ed. 47 (2008) 5806.

Chapter 2

[1] D.B. Williams, C.B. Carter, In Transmission Electron Microscopy; Springer US: Boston, MA, (2009) 3-22

[2] The Unviersity of Iowa, <http://www.uiowa.edu/~cmrf/methodology/sem/index.html> (visited 19 September, 2012).

[3] F. Krumeich, Eletron Microscopy ETH Zurich, http://www.microscopy.ethz.ch/bragg.htm (visited 19 September, 2012)

Chapter 3

[1] Y. Zhao, J.S. Zhang, D.L. Akins, J.W. Lee, Industrial & Engineering Chemistry Research, 50 (2011) 10024.

[2] S. Bonacchi, D. Genovese, R. Juris, M. Montalti, L. Prodi, E. Rampazzo, N. Zaccheroni, Angew. Chem. Int. Ed. 50 (2011) 4056.

[3] M. Roca, A.J. Haes, J. Am. Chem. Soc. 130 (2008) 14273.

[4] Q. He, J.L. Shi, J. Mater. Chem. 21 (2011) 5845.

[5] Y.H. Jin, A. Li, S.G. Hazelton, S. Liang, C.L. John, P.D. Selid, D.T. Pierce, J.X. Zhao, Coordination Chemistry Reviews, 253 (2009) 2998.

[6] F. Caruso, R.A. Caruso, H. MÖhwald, Science 282 (1998) 1111.

[7] Y.D. Yin, R.M. Rioux, C.K. Erdonmez, S. Hughes, G.A. Somorjai, A.P. Alivisatos, Science 304 (2004) 711.

[8] Y.G. Xia, Y.N. Xia, J. Am. Chem. Soc. 126 (2004) 3892.

[9] M.H. Yu, H.N. Wang, X.F. Zhou, P. Yuan, C.Z. Yu, J. Am. Chem. Soc. 129 (2007) 14576.

[10] J.G. Wang, F. Li, H.J. Zhou, P.C. Sun, D.T. Ding, T.H. Chen, Chem. Mater. 21 (2009) 612.

[11] Q.B. Wang, L. Yan, H. Yan, Chem. Commun. (2007) 2339.

[12] L. Zhang, M. D'Acunzi, M. Kappl, G.K. Auernhammer, D. Vollmer, C.M. van Kats, A. van Blaaderen, Langmuir 25 (2009) 2711.

[13] X.W. Lou, L.A. Archer, Z.C. Yang, Adv. Mater. 20 (2008) 1.

[14] W.C. Yoo, A. Stein, Chem. Mater. 23 (2011) 1761.

[15] Y. Yamada, K. Yano, Micropor. Mesopor. Mater. 93 (2006) 190.

[16] H.J. Zhang, J. Wu, L.P. Zhou, D.Y, Zhang, L.M. Qi, Langmuir 23 (2007) 1107.

[17] Z.G. Teng, Y.D. Han, J. Li, F. Yan, W.S. Yang, Micropor. Mesopor. Mater. 127 (2010) 67.

[18] J.C. Zhang, M. Liu, A.F. Zhang, K.F. Lin, C.S. Song, X.W. Guo, Solid State Sci. 12 (2010) 267.

[19] H.N. Zhang, T.J. Bandosz, D.L. Akins, Chem. Commun. 47 (2011) 7791.

[20] H.N. Zhang, Y. Zhou, Y.R. Li, T.J. Bandosz, D.L. Akins, J. Colloid Interface Sci. 375 (2012) 106.

[21] Z.G. Feng, Y.S. Li, D.S. Niu, L. Li, W.R. Zhao, H.R. Chen, L. Li, J.H. Gao, M.L. Ruan, J.L. Shi, Chem. Commun. (2008) 2629.

[22] L.M. Yang, Y.J. Wang, G.S. Luo, Y.Y. Dai, Micropor. Mesopor. Mater. 94 (2006) 269.

[23] Z.A. Qiao, L. Zhang, M.Y. Guo, Y.L. Liu, Q.S. Huo, Chem. Mater. 21 (2009) 3823.

[24] L.L. Hench, J.K. West, Chem. Rev. 90 (1990) 33.

[25] C.J. Brinker, Journal of Non-Crystalline Solids 100 (1988) 31.

[26] S.L. Chen, P. Dong,G.H. Yang, J.J. Yang, Ind. Eng. Chem. Res. 35 (1996) 4487.

[27] T.R. Zhang, J.P. Ge, Y.X. Hu, Q. Zhang, S. Aloni, Y.D. Yin, Angew. Chem. Int. Ed. 47, (2008) 5806.

[28] T.R. Zhang, Q. Zhang, J.P. Ge, J. Goebl, M.W. Sun, Y.S. Yan, Y.S. Liu, C.L. Chang, J.H. Guo, Y.D. Yin J. Phys. Chem. C 113 (2009) 3168.

[29] Q. Zhang, T.R. Zhang, J.P. Ge and Y.D. Yin, Nano Lett. 8 (2008) 2867.

[30] Y. Chen, H.G. Chen, L.M. Guo, Q.J. He, F. Chen, J. Zhou, J.W. Feng, J.L. Shi, ACS Nano 4 (2010) 529.

[31] X. Du, J.H. He, ACS Appl. Mater. Interfaces 3 (2011) 1269.

[32] X.L. Fang, C. Chen, Z H. Liu, P.X. Liu, N.F. Zheng, Nanoscale 3 (2011) 1632.

[33] T. Asefa, Y.J. Shi, J. Mater. Chem. 18 (2008) 5604.

[34] W. Stöber, A. Fink, E. J. Bohn, J. Colloid Interface Sci. 26 (1968) 62.

[35] D.S. Jacob, A. Gedanken, J. Am. Ceram. Soc. 91 (2008) 3024.

[36] J.L. Koenig, Acc. Chem. Res. 14 (1981) 171.

[37] S. Bruynooghe, F. Bertin, A. Chabli, J.C. Gay, B. Blanchard, M. Couchaud, Thin Solid Films 313 (1998) 722.

[38] H. Zhu, Y.G. Ma, Y.G. Fan, J.C. Shen, Thin Solid Films 397 (2001) 95.

[39] V. Bansal, A. Ahmad, M. Sastry, J. Am. Chem. Soc. 128 (2006) 14059.

[40] Z. Lin, J.J. Cai, L.E. Scriven, H.T. Davis, J. Phys. Chem. 98 (1994) 5984.

[41] A. López-Noriega, E. Ruiz-Hernandez, S.M. Stevens, D. Arcos, M.W. Anderson, O. Terasaki, M. Vallet-Regí, Chem. Mater. 21 (2009) 18.

Chapter 4

[1] P.A. Williamson, P.J. Blower, M.A. Green, Chem. Commun. 47 (2011) 1568.

[2] C.T. Kresge, M.E. Leonowicz, W.J. Roth, J.C. Vartuli, J.S. Beck, Nature 359 (1992) 710.

[3] W. Xu, L. Yang, D.L. Akins, J. Phys. Chem. B 106 (2002) 11127.

[4] H.Q. Guo, W. Xu, M.H. Cui, N.L. Yang, D.L. Akins, Chem. Commun. 12 (2003) 1432.

[5] X.M. Zhang, C. Zhang, H.Q. Guo, W.L. Huang, T. Polenova, L.C. Francesconi, D.L. Akins, J. Phys. Chem. B 109 (2005) 19156.

[6] G.M. Andrés, P.J. Jorge, M.L. Luis, Adv. Mater. 22 (2010) 1182.

[7] W. Stöber, A. Fink, E.J. Bohn, J. Colloid Interface Sci. 26 (1968) 62.

[8] M. Grun, I. Lauer, K.K. Unger, Adv. Mater. 9 (1991) 254.

[9] K. Schumacher, P.I. Ravikovitch, A. Du Chesne, A.V. Neimark, K.K. Unger, Langmuir 16 (2000) 4648.

[10] K. Schumacher, M. Grun, K.K. Unger, Microporous Mesoporous Mater. 27 (1999) 201.

[11] Z.G. Teng, Y.D. Han, J. Li, F. Yan, W.S. Yang, Microporous Mesoporous Mater. 127 (2010) 67.

[12] J.C. Zhang, M. Liu, A.F. Zhang, K.F. Lin, C.S. Song, X.W. Guo, J. Solid State Sci. 12 (2010) 267

[13] Y. Yuri, Y. Kasuhisa, Microporous Mesoporous Mater. 93 (2006) 190.

[14] D. Tao, S. Kai, C. Koen, C.H. Tung, Adv.Mater. 21 (2009) 1936.

[15] Y.X. Hu, J.P. Ge, Y.D. Yin, Chem. Commun. 8 (2009) 914.

[16] X.W. Lou, C.L. Yuan, L.A. Archer, Adv. Mater. 19 (2007) 3328.

[17] T.R. Zhang, Q. Zhang, J.P. Ge, G. James, M.W. Sun, Y.S. Yan, Y.S. Liu, C.L. Chang, J.H. Guo, Y.D. Yin, J. Phys. Chem. C 113 (2009) 3168.

[18] J.H. Zhang, H.Y. Liu, Z.L. Wang, N.B. Ming, Chem.-Eur. J. 14 (2008) 4374.

[19] A. Kuijk, A. van Blaaderen, A. Imhof, J. Am. Chem. Soc. 133 (2011) 2346.

[20] H.M. Princen, S.G. Mason, J. Colloid Sci. 20 (1965) 156.

[21] H.M. Princen, S.G. Mason, J. Colloid Sci. 20 (1965) 246.

[22] B.J. Park, E. Furst, Langmuir 26 (2010) 10406.

[23] M. Ryan, J. Fung, D. Kaz, V.N. Manoharan, Materials Today 13 (2010) 34.

[24] B.P. Binks, J.A. Rodrigues, W.J. Frith, Langmuir 23 (2007) 3626.

[25] R. Nagarajan, C.C. Wang, Langmuir 16 (2000) 5242.

Chapter 5

[1] Q.J. He, J.L. Shi, J. Mater. Chem. 21 (2011) 5845.

[2] S. Bonacchi, D. Genovese, R. Juris, M. Montalti, L. Prodi, E. Rampazzo, N. Zaccheroni, Angew. Chem. Int. Ed. 50 (2011) 4056.

[3] G.M. Andrés, P.J. Jorge, M.L. Luis, Adv. Mater. 22 (2010) 1182.

[4] H.Q. Guo, W. Xu, M.H. Cui, N.L. Yang, D.L. Akins, Chem. Commun. 12 (2003) 1432.

[5] X.M. Zhang, C. Zhang, H.Q. Guo, W.L. Huang, T. Polenova, L.C. Francesconi, D.L. Akins, J. Phys. Chem. B 109 (2005) 19156.

[6] M. Roca, A.J. Haes, J. Am. Chem. Soc. 130 (2008) 14273.

[7] Y. Yamada, M. Mizutani, T. Nakamura, K. Yano, Chem. Mater. 22 (2010) 1695.

[8] R.A. Caruso, M. Antonietti, Chem. Mater. 13 (2001) 3272.

[9] L.M. Liz-Marzan, P. Mulvaney, in Surfactant Science Series, ed. U. Zoller, Taylor & Francis, London. 2006.

[10] F. Caruso, R.A. Caruso, H. MÖhwald, Science 282 (1998) 1111.

[11] Y.D. Yin, R.M. Rioux, C.K. Erdonmez, S. Hughes, G.A. Somorjai, A.P. Alivisatos, Science 304 (2004) 711.

[12] Y.G. Sun, Y.N. Xia, J. Am. Chem. Soc. 126 (2004) 3892.

[13] M.H. Yu, H.N. Wang, X.F. Zhou, P. Yuan, C.Z. Yu, J. Am. Chem. Soc. 129 (2007) 14576.

[14] J.G. Wang, F. Li, H.J. Zhou, P.C. Sun, D.T. Ding, T.H. Chen, Chem. Mater. 21 (2009) 612.

[15] J. Liu, S.B. Hartono, Y.G. Jin, Z. Li, G.Q. Lu, S.Z. Qiao, J. Mater. Chem. 20 (2010) 4595.

[16] D. Tao, S. Kai, C. Koen, C.H. Tung, Adv.Mater. 21 (2009) 1936.

[17] Y.X. Hu, J.P. Ge, Y.D. Yin, Chem. Commun. 8 (2009) 914.

[18] A. Kuijk, A. van Blaaderen, A. Imhof, J. Am. Chem. Soc. 133 (2011) 2346.

[19] X.W. Lou, C.L. Yuan, L.A. Archer, Adv. Mater. 19 (2007) 3328.

[20] T.R. Zhang, Q. Zhang, J.P. Ge, G. James, M.W. Sun, Y.S. Yan, Y.S. Liu, C.L. Chang, J.H. Guo, Y.D. Yin, J. Phys. Chem. C 113 (2009) 3168.

[21] T.R. Zhang, J.P. Ge, Y.X. Hu, Q. Zhang, Y.D. Yin, Angew. Chem. Int. Ed. 47 (2008) 5806.

[22] Q. Zhang, T.R. Zhang, J.P. Ge, Y.D. Yin, Nano Lett. 8 (2008) 2867.

[23] Y. Chen, H.G. Chen, L.M. Guo, Q.J. He, F. Chen, J. Zhou, J.W. Feng, J.L. Shi, ACS Nano 4 (2010) 529.

[24] X. Du, J.H. He, ACS Appl. Mater. Interfaces 3 (2011) 1269.

[25] X.L. Fang, C. Chen, Z.H. Liu, P.X. Liu, N.F. Zheng, Nanoscale 3 (2011) 1632.

[26] B. Liu, H.C. Zeng, Small, 5 (2005) 566.

[27] H.N. Zhang, T.J. Bandosz, D.L. Akins, Chem. Commun. 47 (2011) 7791.

[28] W. Stober, A. Fink, E.J. Bohn, J. Colloid Interface Sci. 26 (1968) 62.

[29] M. Grun, I. Lauer, K.K. Unger, Adv. Mater. 9 (1991) 254.

[30] S. Bruynooghe, F. Bertin, A. Chabli, J.C. Gay, B. Blanchard, M. Couchaud, Thin Solid Films 313 (1998) 722.

[31] H. Zhu, Y.G. Ma, Y.G. Fan, J.C. Shen, Thin Solid Films 397 (2001) 95.

[32] Y.L. Shi, T. Asefa, Langmuir 23 (2007) 9455.